ADVANCED ENGINEERING MATERIALS
www.aem-journal.com

Large-Scale Interlaboratory Study Along the Entire Process Chain of Laser Powder Bed Fusion: Bridging Variability, Standards, and Optimization across Metals and Polymers

Ihsan Murat Kuşoğlu, Sunidhi Garg, Arvid Abel, Prasanna V. Balachandran, Stephan Barcikowski, Louis Becker, Jan-Simeon Bernsmann, Jonas Boseila, Christoph Broeckmann, Mert Coskun, Malte Dreyer, Mark East, Mark Easton, Nils Ellendt, Stan Gann, Bilal Gökce, Mareen Goßling, Joachim Greiner, Piotr Gruber, Moritz Grünewald, Kopila Gurung, Nick Hantke, Florian Hengsbach, Hannes Holländer, Brecht Van Hooreweder, Kay-Peter Hoyer, Yajiang Huang, Florian Huber, Olaf Kessler, Burçin Özbay Kısasöz, Stefan Kleszczynski, Ebubekir Koc, Tomasz Kurzynowski, Arno Kwade, Simon Leupold, Dongmei Liu, Felix Lomo, Arne Lüddecke, Gerrit A. Luinstra, David A. Mauchline, Fabian Meyer, Lars Meyer, Peter Middendorf, Stefan Nolte, Michał Olejarczyk, Ludger Overmeyer, Andrij Pich, Sebastian Platt, Felix Radtke, Roland Ramm, Silja-Katharina Rittinghaus, Richard Rothfelder, Johannes Rudloff, Mirko Schaper, Marie Luise Scheck, Johannes Henrich Schleifenbaum, Michael Schmidt, Jan T. Sehrt, Yvonne P. Shabanga, Alexander Sommereyns, Rabea Steuer, Layla Shams Tisha, Anastasiya Toenjes, Christopher Tuck, Adrian Vaghar, Bey Vrancken, Zhengze Wang, Sebastian Weber, Jan Wegner, Bai-Xiang Xu, Yangyiwei Yang, Duyao Zhang, Evgeny Zhuravlev, and Anna R. Ziefuss*

I. M. Kuşoğlu, S. Barcikowski, S. Gann, A. R. Ziefuss
Technical Chemistry I and Center for Nanointegration Duisburg-Essen (CENIDE)
University of Duisburg Essen
45141 Essen, Germany
E-mail: stephan.barcikowski@uni-due.de

S. Garg, P. V. Balachandran
Department of Materials Science and Engineering
University of Virginia
Charlottesville, VA 22902, USA

A. Abel, H. Holländer
Additive Manufacturing Department
Laser Zentrum Hannover e.V. (LZH)
D-30419 Hannover, Germany

L. Becker, S. Weber
Chair of Materials Technology
Ruhr University Bochum
44801 Bochum, Germany

J.-S. Bernsmann, J. Boseila, J. H. Schleifenbaum
Digital Additive Production DAP
RWTH Aachen University
Campus-Boulevard 73, 52074 Aachen, Germany

C. Broeckmann, F. Radtke, M. L. Scheck
Institute of Applied Powder Metallurgy and Ceramics (IAPK)
RWTH Aachen e.V.
52062 Aachen, Germany

M. Coskun, B. Ö. Kısasöz, E. Koc
ALUTEAM
Fatih Sultan Mehmet Vakıf University
34421 Istanbul, Turkey

M. Dreyer, F. Hengsbach, K.-P. Hoyer, M. Schaper
Chair of Materials Science
Paderborn University
33098 Paderborn, Germany

M. East, C. Tuck
Centre for Additive Manufacturing
Faculty of Engineering
University of Nottingham
Nottingham NG7 2RD, UK

The ORCID identification number(s) for the author(s) of this article can be found under https://doi.org/10.1002/adem.202402930.

DOI: 10.1002/adem.202402930

Laser powder bed fusion is a cornerstone technology for additive manufacturing (AM) of metals and polymers, yet challenges in achieving consistent reproducibility and process optimization persist. Addressing these requires a systematic understanding of the interactions between feedstock, process parameters, and final part characteristics throughout the entire production chain. This study presents results from a comprehensive interlaboratory investigation conducted by 32 research institutions, evaluating six feedstock, including nanoparticle-modified aluminum alloy and polyamide powders, under standardized protocols. Data analysis encompasses 69 powder properties, 15 process parameters per print, and 78 part features, culminating in a dataset of over 1.2 million correlations. Advanced statistical methods and machine learning are employed to identify critical variability drivers, such as the impact of nanoparticle modifications on powder flowability and thermal conductivity, as well as the influence of process parameters on reproducibility. Newly introduced dimensionless figures of merit provide universal metrics to describe and predict thermal and mechanical interactions, simplifying process optimization and material characterization. The findings, supported by an open-access dataset adhering to findable, accessible, interoperable, and reusable principles, advance understanding of material–process–structure–property relationships. They establish a benchmark for future research and lay the foundation for improving the reliability, quality, and sustainability of AM processes.

1. Introduction

Laser powder bed fusion (PBF-LB) of metals and polymers has revolutionized industrial production through rapid, customized part manufacturing.[1–5] While this technology has reached a high technical readiness level, understanding and controlling the complex interdependencies along the process chain remains a significant challenge.[6,7] This is especially critical in industries such as aerospace,[8] automotive,[9] and medical,[10] where tailored material properties, precision, and part performance are crucial. Variations in machine calibration, process parameters, operator skills, and material/feedstock properties introduce complexity, affecting key outcomes such as dimensional accuracy, mechanical strength, surface finish, and microstructure.[11–13] Addressing these challenges requires a systematic approach, investigating how feedstock properties and processing conditions influence part quality, focusing on developing robust methodologies, and understanding the underlying mechanisms.[7,14,15]

M. Easton, F. Lomo, D. Zhang
Centre for Additive Manufacturing
School of Engineering
RMIT University
Melbourne, VIC 3000, Australia

N. Ellendt, L. S. Tisha, A. Toenjes
Leibniz Institute for Materials Engineering - IWT
28359 Bremen, Germany

N. Ellendt, L. S. Tisha, A. Toenjes
Faculty of Production Engineering
University of Bremen
Badgasteiner Straße 1, 28359 Bremen, Germany

B. Gökce, M. Goßling, S.-K. Rittinghaus, M. Schmidt
Chair of Materials Science and Additive Manufacturing
School of Mechanical Engineering and Safety Engineering
University of Wuppertal
42119 Wuppertal, Germany

J. Greiner, P. Middendorf
Institute of Aircraft Design
University of Stuttgart
70569 Stuttgart, Germany

P. Gruber, T. Kurzynowski, M. Olejarczyk
Department of Laser Technologies
Automation and Production Organization
Faculty of Mechanical Engineering
Wroclaw University of Science and Technology
Wyb. Wyspiańskiego 27, 50–370 Wrocław, Poland

M. Grünewald, J. Rudloff
SKZ-KFE gGmbH
Friedrich-Bergius-Ring 22, 97076 Würzburg, Germany

M. Grünewald
Fraunhofer Institute for Manufacturing Engineering and Automation IPA
Nobelstraße 12, 70569 Stuttgart, Germany

K. Gurung, B. Van Hooreweder, B. Vrancken
Department of Mechanical Engineering
KU Leuven
3001 Leuven, Belgium

K. Gurung
Flanders Make@KU Leuven
3001 Leuven, Belgium

N. Hantke, J. T. Sehrt
Hybrid Additive Manufacturing
Ruhr University Bochum
44801 Bochum, Germany

Y. Huang, Z. Wang
College of Polymer Science and Engineering
State Key Laboratory of Advanced Polymer Materials
Sichuan University
Chengdu 610065, China

F. Huber, S. Leupold, R. Rothfelder, A. Sommereyns
Institute of Photonic Technologies
Friedrich-Alexander-Universität Erlangen-Nürnberg
91052 Erlangen, Germany

O. Kessler, R. Steuer, E. Zhuravlev
Chair of Materials Science
Faculty of Mechanical Engineering and Marine Technology
Rostock University
18051 Rostock, Germany

As these determinants are interrelated along the process chain, from feedstock micropowder properties to the final printed part, these challenges can only be properly addressed if property metrics are tracked in all steps. Standard operating procedures (SOPs) for feedstock preparation, including the additivation of nanoparticles (NPs), as well as methods for process and part characterization, are essential to identify relevant influencing factors. Such a comprehensive approach paves the way for optimizing PBF-LB processes and advancing the capabilities of this transformative technology. Interlaboratory studies (ILSs) provide a framework for systematically investigating the interdependencies between feedstock properties, process parameters, and part outcomes across diverse conditions and setups, enabling deeper insights into the mechanisms governing the PBF-LB process and supporting the development of standardized methodologies. ILSs are collaborative studies that enhance result quality through analyses performed by multiple laboratories on a common test material.[16] An ILS goes beyond focused-purpose activities such as method-performance studies (also known as Round Robin), laboratory-performance studies (proficiency testing), or material-certification studies.[17–21] By fostering a collaborative framework, ILSs help to assess and improve the performance, precision, and reliability of additive manufacturing (AM) processes but also may scientifically address interrelations along the material-process-part-chain. Furthermore, such studies hold the potential to uncover hidden correlations between variables that have not yet been described in the literature, providing new insights into the complexities of the process and opportunities for optimization.[22,23] To realize the potential of an ILS, a study design is required that ideally considers and tracks all material, experimental, and procedural determinants of the studied process chain. In the context of PBF-LB, where higher product consistency and quality are imperative, only Round Robins or lab-performance studies have been conducted. Most of these studies focus on either metal or polymer processing, highlighting the variability of individual process steps, such as roughness, corrosion resistance, and flowability.[24–26] However, these studies primarily evaluated centralized manufacturing plans or machine manufacturer guidelines, often overlooking the influence of raw feedstock materials on part properties. While there are studies examining the entire process chain for either polymer or metals,[27–29] to the best of our knowledge, they have not yet investigated both material types (polymers and metals) in a single ILS all along the entire process chain. This gap is particularly intriguing, as studying both materials together could uncover unexplored insights into process optimization and consistency. An ILS that fully incorporates research data management (RDM) standards and examines the entire PBF-LB process chain provides a holistic view of the interdependencies between feedstock properties, processing parameters, and final part performance. It provides valuable insights into how feedstock characteristics influence outcomes and support optimizing commercially available and NP-modified feedstocks. In recent years, feedstock modification has gained significant attention, particularly through the surface decoration of commercial feedstocks with NPs.[30–34]

O. Kessler, R. Steuer, E. Zhuravlev
Competence Center CALOR, Department Life, Light and Matter, Interdisciplinary Faculty
Rostock University
18051 Rostock, Germany

S. Kleszczynski, L. Meyer, S. Platt, J. Wegner
Chair of Manufacturing Technology
Institute for Product Engineering
University of Duisburg-Essen
47057 Duisburg, Germany

S. Kleszczynski, J. Wegner
Center for Nanointegration Duisburg-Essen (CENIDE)
47057 Duisburg, Germany

E. Koc
Department of Industrial Engineering
Boğaziçi University
34342 Istanbul, Turkey

A. Kwade, A. Lüddecke
Technische Universität Braunschweig
Institut für Partikeltechnik
38104 Braunschweig, Germany

D. Liu, S. Nolte
Institute of Applied Physics
Abbe-Center of Photonics
Friedrich–Schiller–Universität Jena
07745 Jena, Germany

G. A. Luinstra, A. Vaghar
Institute of Technical and Macromolecular Chemistry
University Hamburg
20146 Hamburg, Germany

D. A. Mauchline, Y. P. Shabanga
Vaal University of Technology
Southern Gauteng Science and Technology Park
Private Bag X021, Vanderbijlpark 1900, South Africa

F. Meyer, A. Pich
DWI Leibniz Institut
RWTH Aachen University
52074 Aachen, Germany

S. Nolte, R. Ramm
Fraunhofer Institute for Applied Optics and Precision Engineering IOF
07745 Jena, Germany

L. Overmeyer
Produktionstechnisches Zentrum Hannover
Institut für Transport- und Automatisierungstechnik
Gottfried Wilhelm Leibniz Universität Hannover
30823 Garbsen, Germany

B.-X. Xu, Y. Yang
Mechanics of Functional Materials Division
Institute of Materials Science
Technische Universität Darmstadt
64287 Darmstadt, Germany

D. Zhang
Department of Mechanical Engineering
University of Bath
BA2 7AY Bath, UK

These NP-modified feedstocks are becoming increasingly prominent in research and development due to their potential to enhance powder properties, processing efficiency, microstructure, and, ultimately, the performance of final parts produced in PBF-LB.[35–38] In this field of work, numerous studies focus on NP-based feedstock modification, but very few investigate the influence of NPs across the entire PBF-LB process chain.[39–48]

Understanding how NP modifications impact not just the powder but each process stage—from powder handling to part performance—remains an underexplored area with significant potential for optimizing AM outcomes. Kusoglu et al. recently proposed an ILS design that included investigating the quantified effects of feedstock modification on metal and polymer characteristics, process behavior, microstructure, and part properties in the PBF-LB, including aspects like repeatability, reproducibility, and RDM under findable, accessible, interoperable, and reusable (FAIR) principles.[49] They proposed investigating six different feedstocks, including AlSi10Mg alloy and polyamide-12 (PA12), both in their commercial and modified forms, across the entire PBF-LB process chain. These commercial materials are widely regarded as the gold standards for polymer and metal PBF-LB, respectively. AlSi10Mg and PA12 are extensively studied in PBF-LB research and are widely utilized in industrial applications. The nanoadditivation of these feedstocks is not primarily aimed at enhancing mechanical properties through grain refinement or crystallization. Instead, it seeks to investigate the compatibility of nanoadditivated feedstock variants with the PBF-LB process. Specifically, this approach examines the robustness of PBF-LB against NP incorporation, which is of particular importance for the AM of nanofunctionalized components.

The current study follows the design published by Kusoglu et al.[49] executed across 32 nonprofit research organizations along the scheme summarized in **Figure 1**. Six different feedstocks were processed using 20 PBF-LB machines, evenly split between metals (10 machines) and polymers (10 machines). In total, 69 powder features (39 for metals and 30 for polymers) and 78 part features (46 for metals and 32 for polymers) were measured. Note that this results in a cumulative total of over 500 000 correlations involving metals and polymers, extracted to over 1 200 000 correlations when including replicates. For example, the powder particle size histogram consists of a hundred 2D data points that represent a single feature, and its detailed analysis allows the extraction of multiple parameters, such as the d_{10}, d_{50}, and d_{90} values, as well as the span. Since each histogram was measured in triplicate, this greatly increases the number of parameters and potential correlations in the dataset. The prospect of a rich dataset that arose during the study's design motivated adequate data acquisition and handling standardization.

Consequently, our study implemented a comprehensive RDM grounded in the FAIR principles, which required the study partners to agree on SOPs for the experimental and RDM execution. Adhering to these SOPs, the research aimed to understand the PBF-LB process comprehensively. The study also quantified the uncertainties in powder properties, PBF-LB process parameters, and as-built part features for both commercial and NP-modified polymer and metal feedstocks using relative standard deviations (RSD). This approach provided valuable insights into the reproducibility, or lack thereof, across the entire PBF-LB process chain.

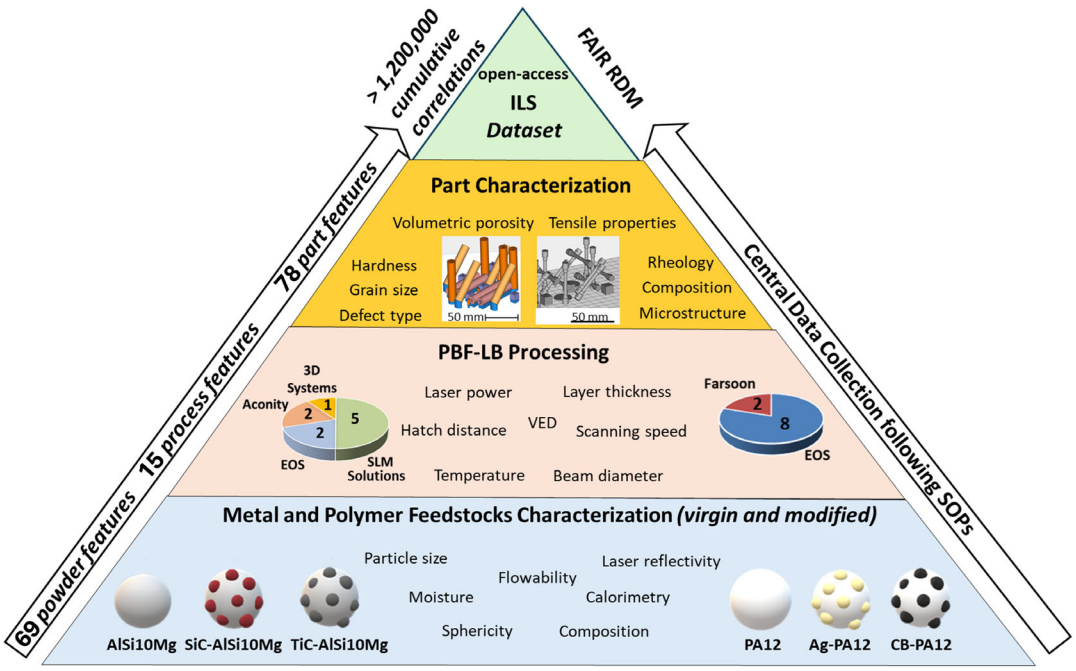

Figure 1. Graphical illustration of the overall study design collecting FAIR data along the entire process chain of the PBF-LB process ILS dataset for three metal powder compositions (AlSi10Mg, SIC–AlSi10Mg, and TiC–AlSi10Mg) involving 39 powder, 7 process, and 46 part features, and for three polymer powder compositions (PA12, Ag-PA12, and CB-PA12) involving 30 powder, 8 process, and 32 part features. Note that the cumulative correlations include repeated measurements as conducted within this study.

This large-scale ILS effort generated extensive, high-dimensional data, which was analyzed using principal component analysis (PCA) and machine learning (ML) models (details given in the Experimental Section). As an overall outcome, new dimensionless figures of merit are developed, which support simplifying the PBF-LB process and generalizing its complex physical phenomena by reducing the number of variables.[50] While statistical and ML models uncovered hidden correlations, identified key variability drivers, and detected outliers, dimensionless figures of merit provide a way to characterize physical phenomena and compare different materials and conditions. The outcomes of this study offer crucial insights into the factors influencing part properties in PBF-LB, serve as a guide for optimizing the complex PBF-LB process, and tell about the robustness of this AM method toward nanofunctionalized 3D printing. Additionally, the open-access FAIR data enable further data-driven analyses and ML, driving progress in AM technologies.

2. Results and Discussion

The basis for reproducibility, repeatability, statistical correlation analysis, ML, and dimensionless figures of merit analysis discussed in this section is the open-access ILS dataset published under FAIR principles.[51] First, the reproducibility and repeatability of the powder properties, PBF-LB processing conditions, and part properties are assessed to ensure reliability by quantifying the relative variability across different settings and operators. Essentially, the term relative variability refers to estimating how sensitive a part property is to slight changes in the processing conditions and powder properties in PBF-LB. Next, PCA is performed on the powder properties dataset (both metals and polymers) to reduce the dimensionality of the dataset and uncover hidden correlations. The outcomes from PCA are used to identify and interpret key differences in the powder features (Figure 1) between commercial and NP-modified feedstocks, which subsequently influence the part properties. Since PBF-LB processing conditions are critical to model the part properties, ML methods are used to establish a quantitative relationship between the powder properties (an outcome from PCA), PBF-LB processing conditions, and part properties. Note that the dataset[51] includes a wealth of additional parameters, such as data on used powder and heat-treated samples, which were not analyzed in this study for the sake of focus and clarity. These data are, however, available to the community for further exploration and analysis. Furthermore, only the core measurement methods are discussed in this section. Detailed descriptions of the methodologies, including all measured parameters, their respective units, allowed ranges, and specific measurement protocols, can be found in the respective SOPs.[52] Finally, four dimensionless figures of merit were developed that provide a universal basis for identifying relationships, such as how material and process parameters systematically influence part performance, and for defining corridors or best effort guidelines. By simplifying complex relationships, they serve as a powerful tool for decision making.

2.1. Reproducibility and Repeatability

ILSs are also critical for ensuring data reliability, especially in complex manufacturing processes like PBF-LB. To achieve consistent and trustworthy results, validating the repeatability and reproducibility of the entire PBF-LB process chain is essential. Repeatability refers to the consistency of measurements under identical conditions, while reproducibility assesses how results vary across different settings and operators. This validation helps to identify the dataset's strengths and potential weaknesses, ensuring that the data is robust and suitable for further analysis and process optimization. RSD is a key metric used to extract information on both repeatability and reproducibility. It offers a standardized measure of data variability relative to its mean, which facilitates a clearer understanding of measurement consistency. Generally, a lower RSD indicates high consistency and reliability, while a higher RSD suggests greater variability, highlighting areas where process or measurement variability may need to be addressed.[53] **Figure 2** illustrates the RSD of features assessed experimentally across the entire process chain, encompassing powder, process, and part properties for both metals and polymers. For both material systems, powder properties

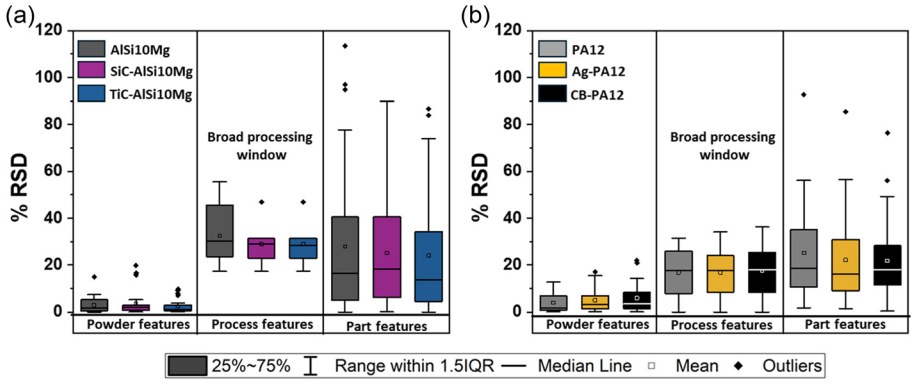

Figure 2. Illustration of the RSD calculated via %RSD = $(s \times 100)/(x)$ with s = standard deviation and x = mean value, observed across all parameters assessed throughout the PBF-LB process chain for both NP-modified and unmodified feedstocks. a) Metal feedstocks: The RSD was averaged over 39 powder, 7 process, and 46 part properties. b) Polymer feedstocks: The RSD was averaged over 30 powder, 8 processes, and 32 part properties. See Table 2 and 3 in the Experimental Section that lists all powder and process features evaluated in the study, separated by material class (metals and polymers).

exhibited the highest repeatability compared to process and part properties. In metals (Figure 2a), the powder properties of NP-modified feedstocks showed a tighter RSD distribution than commercial AlSi10Mg powders. Conversely, in polymers (Figure 2b), the repeatability of powder properties was slightly lower than that of metals, with NP modification only marginally improving the RSD over commercial PA12 powders. In contrast, the part properties exhibited a wider range of RSD for both metals and polymers (see right panels in Figure 2a,b, as well as Figure S1 and S2 (SI) for the evaluated powder and process features). This variability is primarily attributed to differences in the PBF-LB process parameters used by ILS participants. Each participant followed a defined process parameter corridor specified in their respective SOPs.[52] However, differences across groups and machines led to a broader process window (see middle panels in Figure 2a,b), resulting in higher RSD values for the measured part properties. For example, the SOPs recommended best effort values within an allowed range[52] for the PBF-LB energy density, calculated as (laser power) / (scan speed $\times$ hatch spacing $\times$ powder layer thickness). These values were 0.3 J mm^{-3} (within a range of 0.3–0.45 J mm^{-3}) for polymers and 34 J mm^{-3} (within 20–100 J mm^{-3}) for metals, naturally resulting in some variability in the RSD (see Table S1 and S2 (Supporting Information) for process parameter sets of ILS participants).

Importantly, repeatability—the ability to obtain the same results under identical conditions —was high for both commercial and NP-modified powders, indicating strong consistency in their powder properties (see Figure S1 in the Supporting Information). In contrast, reproducibility—the consistency of results across different operators or laboratories—was influenced by variations in processing parameters among ILS participants. Notably, the influence of NP modifications and feedstock types on part property variations appeared weaker than the impact of processing parameters. Among the part properties analyzed, volumetric pore size distribution and elongation had the highest RSD values (see Figure S2 of the Supporting Information), highlighting the effect of the processing window on part variability.

While powder analysis proved highly repeatable, the reproducibility of part properties in this study is limited by the variation in processing parameters. The narrower processing window for polymers contributed to significantly lower RSD values for their part properties compared to metals, demonstrating better consistency in properties under similar processing conditions. To account for variability across laboratories, the ILS employed various types of PBF-LB machines, each requiring specific process parameter optimization to achieve the acceptance criteria: a density of over 99% for metals and 90% for polymers. These criteria, combined with a "best effort" approach for parameter selection within defined corridors, were essential for enabling meaningful comparisons across participants and laboratories.

Overall, these findings underscore the necessity of careful process parameter selection and control in PBF-LB to enhance both repeatability and reproducibility. These findings present valuable insights for utilizing data generated from the completed ILS. Reliable data derived from reproducible measurements are crucial for establishing robust benchmarks and guidelines for the PBF-LB process. While SOPs were employed to promote consistency and minimize RSD by predefining allowed parameter corridors, some variability in processing parameters is unavoidable in an international study with different machines, underscoring the importance of understanding these factors when evaluating the results.

The overall data quality generated in this ILS provides a strong foundation for further analyses, including PCA and ML, which can uncover deeper relationships between powder properties, PBF-LB processing conditions, microstructure, and part properties. Compared to existing studies on repeatability and reproducibility in PBF-LB, the results of this ILS align with expectations for such a diverse and wide-ranging study. For example, prior research has reported RSD values for metal powder properties typically below 5% for parameters like particle size distribution and flowability, with slightly higher variability (up to 10%) for polymers due to their higher sensitivity to environmental conditions.[54] The powder RSD values in this study are consistent with these benchmarks, particularly for NP-modified powders, which exhibited high repeatability and tighter distributions compared to commercial feedstocks. This highlights the robustness of our powder preparation methodologies and suggests that they can serve as reliable baselines for further investigations. In terms of part properties, previous studies have documented RSD values between 10% and 30% for key metrics like density, tensile strength, and elongation at break, depending on the material and process parameters evaluated.[22,53,55–58] The higher RSD values observed in this ILS for part properties—particularly in metals—can be attributed to the broader process parameter corridors allowed in the study, reflecting the diversity in machine types and operator expertise across participating laboratories. Despite this, the narrower process windows for polymers resulted in RSD values that fall closer to the lower range of reported literature values, indicating better reproducibility under controlled conditions.

The observed repeatability and reproducibility are commendable considering the wide scope of this ILS, including international participants, various machine configurations, and both commercial and NP-modified feedstocks. The results demonstrate that while variability is unavoidable in such a comprehensive study, the data remain sufficiently robust for further evaluation. In particular, the findings emphasize the importance of understanding the interplay between processing parameters and material properties to optimize the PBF-LB process. Compared to other ILSs or repeatability analyses in the field, this study uniquely integrates both metals and polymers while investigating the impact of NP modifications on feedstock performance. Although the reproducibility of part properties for metals may appear lower, this is largely due to the broader process parameter ranges permitted in this study. For instance, RSD values exceeding 20% were observed for rheological features, volumetric pore size distributions, and tensile test elongation (Figure S2, Supporting Information). While this variability presents challenges, it also provides valuable insights into the sensitivity of PBF-LB part properties to process conditions, highlighting the importance of tighter parameter controls to ensure consistent results. In conclusion, the data quality achieved in this ILS is comparable to or better than similar studies in the field,[7,14,18,23] as demonstrated by its adherence to SOPs, comprehensive reporting of PBF-LB process parameters, and rigorous application of FAIR principles. Specifically, the

study's scope—encompassing both metals and polymers—and the generation of over 1.2 million traceable correlations across 69 powder features, 15 process parameters, and 78 part properties surpass comparable ILSs in scale and detail. These aspects underscore the study's relevance as a benchmark for PBF-LB research and its potential to inform best practices for process parameter selection, feedstock design, and material performance evaluation. Furthermore, the robust dataset provides a solid foundation for advanced analyses using PCA and ML, extracting actionable insights and deepening the understanding of PBF-LB processes.

2.2. Capturing Statistical Correlations in the Powder Properties via PCA

The powder feedstock properties are the starting point of the process chain and influence all subsequent steps during PBF-LB, so a closer look at the commercial and nanomodified feedstock material is indispensable. PCA is used to analyze the powder data of metals and polymers within the ILS. PCA is a linear data dimensionality reduction method to extract meaningful information from high-dimensional datasets.[59,60] It assumes that there are several statistically correlated variables in the high-dimensional dataset. It accomplishes the goal by calculating new latent variables called PCs obtained as linear combinations of the original variables with different weights in each PC. The first PC (PC1) captures the most significant variance in the high-dimensional dataset; the second PC (PC2) is orthogonal to PC1 and captures the second largest variance and so on (see the Experimental Section for details). By reducing the dimensionality, PCA highlights the most significant variables contributing to data variability, facilitating a more straightforward interpretation and identification of underlying patterns.[59,60]

Furthermore, PCA aids in comparing different material systems (commercial or NP-modified), enhancing the understanding of their properties and behaviors (shown in Figure S3 for metals and S4 for polymers in Supporting Information). The insights from PCA support decision-making regarding powder material selection and process optimization in the PBF-LB process chain, improving data quality and standardization across laboratories. The metal powder dataset is composed of 30 observations (10 commercial powders, 10 modified by TiC NPs, and 10 modified by SiC NPs), where each observation is represented by 34 features that capture the powder properties. Similarly, the polymer powder dataset comprises 30 observations (10 commercial powders, 10 modified by Ag NPs, and 10 modified by carbon black (CB) NPs), representing each observation by 31 features that capture the powder properties. For example, the polymer dataset contains observations of commercial PA12, Ag-PA12, and CB-PA12 feedstocks, which are, in turn, represented by the features of flowability (using four different flowability test methods), moisture content, laser reflectance, particle size distribution, morphology, and fast scanning calorimetry. **Figure 3**a shows the cumulative variances captured by the PCs on both metal and polymer feedstock datasets.

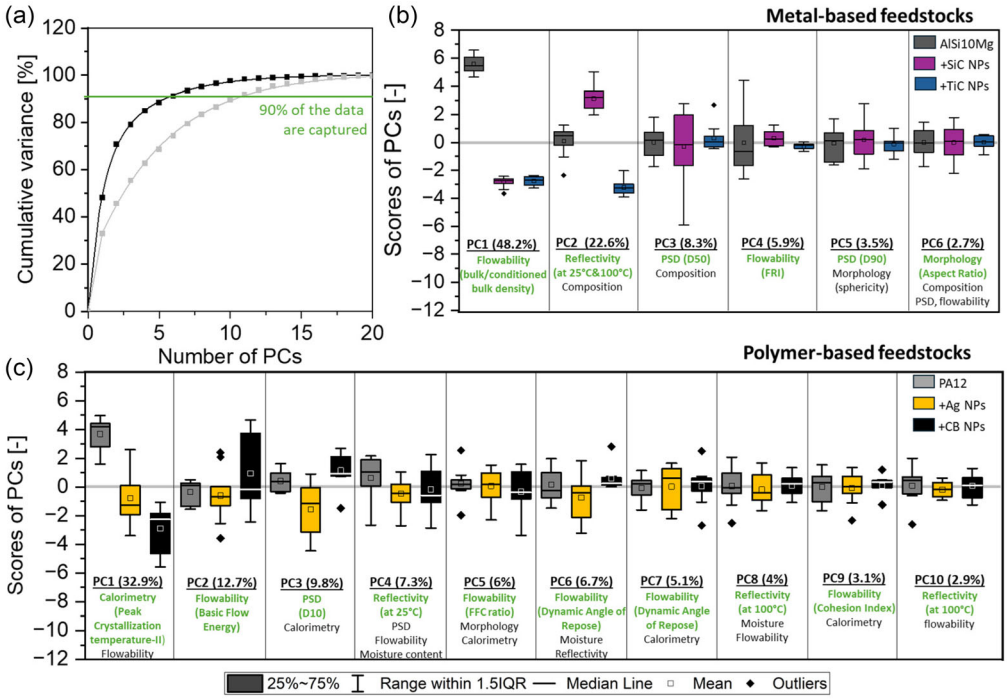

Figure 3. a) Cumulative variance for the different PCs, describing metal (black) and polymer (gray) powder properties. Horizontal green line marks the threshold where the PCs capture 90% of the total variance in the datasets (6 PCs for metals and 10 PCs for polymers). Note that the input data for PCA comes from NP-modified and commercial powder properties. b) First 6 PC scores of the metal feedstock properties. c) First 10 PC scores of the polymer feedstock properties. In b) and c), only those powder properties with loadings exceeding |0.24| are given below each PC, and the features that statistically carry the highest weights are highlighted in green color (see Table S1 and S2 (Supporting Information) for further details).

For metals, six PCs captured ≈90% of the cumulative variance in the dataset, while the polymer dataset required ten PCs to achieve the same threshold. This 90% threshold was chosen based on the maximum estimated RSD of ≈10% for powder properties, as shown in the left panel of Figure 2a. The remaining variance is assumed to result from noise inherent to the wide-scale ILS approach, including variations in measurement techniques, calibration procedures, allowed parameter ranges, and intrinsic stochasticity. Each PC is a linear combination of features describing powder properties (33 for metals, 31 for polymers), with the associated weights (loadings) indicating the relative contribution of each descriptor. To simplify the interpretation and reduce the impact of noise from features with lower absolute weights, only features with absolute weights greater than |0.24| were considered. This threshold was chosen based on an analysis of the distribution of the loading, ensuring a balance between capturing significant contributions and minimizing noise from less relevant features. The dominant powder properties for each PC are indicated in Figure 3b,c for metals and polymers, respectively, with the features highlighted in green representing the highest absolute weights. Detailed PCA loadings for each PC, quantifying the contribution of individual powder descriptors, are provided in Table S3 and S4 in the Supporting Information. Key results of PC score correlations are visualized in Figure S3 (SI) for metal powders and Figure S4 (SI) for polymer powders, showing the PC data clustering of commercial and nanomodified feedstocks processed on different machines.

2.2.1. PCA of Metal Feedstocks

The six PCs extracted from the metal powder dataset are interpreted. Notably, the effects of NP modification are most strongly captured by PC1 and PC2 (Figure 3b), which are dominated by conditioned bulk density (PC1) and reflectivity (PC2). To understand these correlations, both dominant factors were examined in detail (**Figure 4**a,b), revealing differences between commercially and NP-modified powders. Both modified feedstocks exhibit increased bulk density compared to commercial AlSi10Mg powders, caused by tighter packing of powder particles due to a reduction in cohesive interparticle forces (e.g., van der Waals or capillary interactions), which facilitates improved powder flowability and packing density—and, consequently, higher as-built part density.[29,61,62]

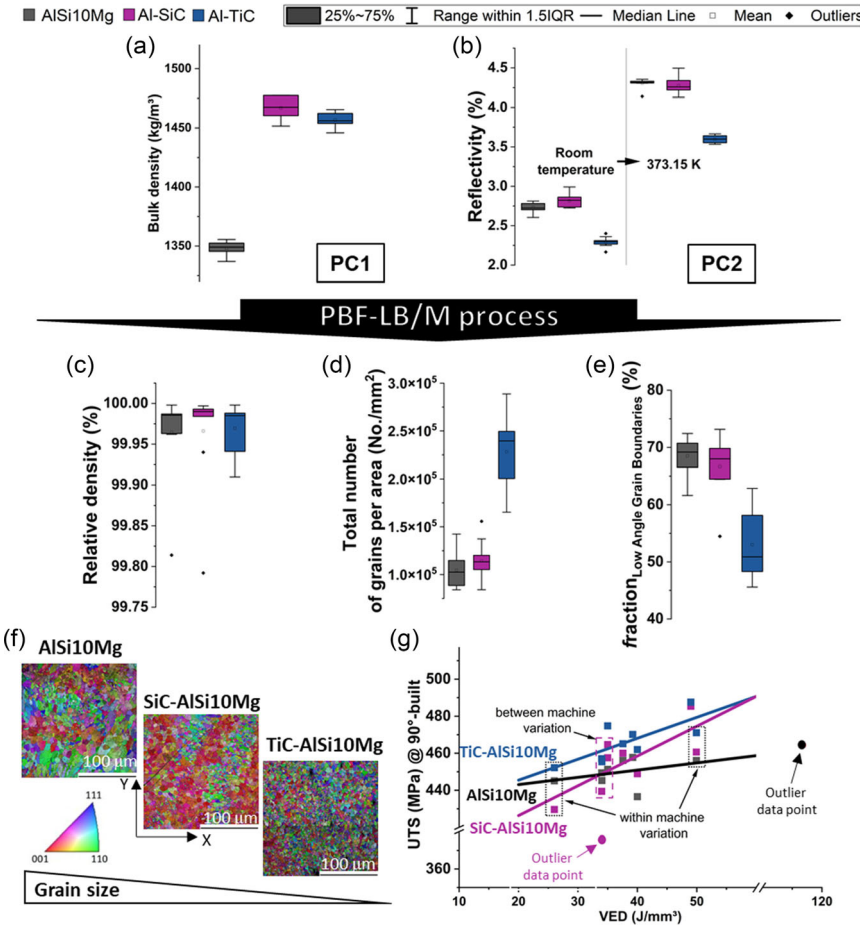

Figure 4. Powder properties of AlSi10Mg-based feedstocks: a) conditioned bulk density and b) reflectivity; and structural properties of as-built parts: c) relative density, d) number of grains mm^{-2}, e) fraction of LAGBs with a region of interest of $\approx 200 \times 200\ \mu m^2$, f) Scanning Electron Microscopy-Electron backscatter diffraction (SEM–EBSD) images measured in *x*–*y* direction, and g) UTS in the vertical build direction for the studied VED range. Mechanical testing of aluminum alloy samples has been performed in the as-built and at least four weeks naturally aged state.

In Figure 4c, the relative part density was plotted to verify this hypothesis, and higher densification, with a narrower deviation between machines, was observed for the SiC NP-modified parts. Interestingly, the relative density of the TiC NP-modified samples remains comparable to that of the part printed from commercial feedstock. This observation may be attributed to the specific interactions of TiC particles with the matrix during the melting process, which might not enhance densification as effectively as anticipated due to instabilities in viscosity, wettability, and liquid–solid rheological properties.[63] However, Pannitz et al. and Lüddecke et al. showed that nanomodification, depending on the material type, decreases the reflectivity of feedstock but is not the only decisive factor for the prevailing temperatures in the powder bed and melt pool; instead, together with improved thermal conductivity, it is an assessing factor significantly influencing process parameter selection and densification during processing.[62,64,65] Despite the increased bulk density (Figure 4a), which is particularly relevant at the start of the scan vector, the significant decrease in reflectivity (Figure 4b) after TiC modification highlights changes in light–particle interactions that additionally influence the final part density and structural properties.[66]

PC2 captures 22.6% of the variance from the dataset, with high contributions from reflectivity. Visualizing the scores of PC2 (shown in Figure 3b) reveals that the TiC NP-modified metal feedstocks behave differently from those of the commercial and SiC NP-modified ones. As reflectivity is the main driver of PC2, the reflectivity for the different feedstocks was plotted (Figure 4b). As expected, the TiC NP-modified metal feedstock shows lower reflectivity at both 298 and 398 K compared to commercial and SiC NP-modified feedstocks (Figure 4b). This lower feedstock reflectivity correlates with increased energy absorption at the start of the scan vector and during the PBF-LB process, where the VED is precompensated to avoid excess heating of the melt pool, promoting more rapid solidification due to higher cooling rates. Such conditions can decrease grain sizes and the microstructure's fraction of low-angle grain boundaries (LAGBs) (f_{LAGB}).[67] It is important to note that PBF-LB involves high cooling rates (10^4–10^6 $K\,s^{-1}$), which strongly influence grain formation. In standard PBF-LB of AlSi10Mg, grains are often columnar, aligned along the thermal gradient due to epitaxial growth. However, in some regions (e.g., near melt pool boundaries), equiaxed grains can form due to local undercooling. Without NP-TiC modification, PBF-LB of AlSi10Mg predominantly has columnar grains with LAGBs and some equiaxed regions with high-angle grain boundaries (HAGBs). Thus, the TiC-NP modification refines grains and increases nucleation sites leading to more equiaxed grains with random orientations and subsequently more HAGBs.[68] While the TiC NP-modified powders did not enhance the relative volumetric density (Figure 4c), this nanoadditive significantly increased the number of grains (Figure 4d), reduced the f_{LAGB} (Figure 4e), and decreased the grain size (Figure 4f). Note that the overall grain size appears smaller than the values commonly described in the literature for this material.[40,66] However, this discrepancy can be attributed to the measurement method, as we analyzed the grain size exclusively in the *xy*-plane, which tends to capture finer grain structures due to the layer-wise nature of the PBF-LB process. These factors collectively contributed to higher ultimate tensile strength (UTS) of the TiC NP modificated prints than found in prints from commercially and SiC NP-modified feedstocks.

2.2.2. PCA of Polymer Feedstock

We focus on interpreting the first ten PCs associated with the polymer powder dataset. The effect of NP modification on the powder properties is evident in the first three PCs (see Figure 3c), which will be discussed in detail. PC1 captures 32.9% of the total variance in the polymer powder dataset, with the second crystallization temperature being the primary contributor. The addition of NPs acts as nucleation sites or restricts chain mobility, facilitating crystallization at slightly lower temperatures during the later stages of powder bed cooling. This influence is reflected in the second crystallization peak, as seen in **Figure 5**a. Differences in nucleation kinetics and NP–polymer chain interactions likely enhance the 3D growth of lamellae to spherulites, creating ellipsoidal crystalline structures.[69,70] It can be hypothesized that this tuned crystalline structure and crystallinity contribute to enhanced mechanical properties in the as-built parts, such as increased strength.[71,72] Figure 5f shows that the UTS in the horizontal direction clearly benefits from NP modification. However, this improvement depends on achieving a balanced crystalline structure, as excessive crystallinity could reduce the elongation and make the material brittle. PC2 accounts for 12.7% of the variance in the dataset and is dominated by the basic flowability energy (BFE), flow rate index (FRI), dynamic angle of repose (DAoR), and Carr index. All these features provide insights into the overall flow behavior of feedstocks. Still, BFE additionally offers information on the compressibility of the feedstocks under dynamic forces via the screw feeder of the test setup. NP modification enhances flowability and bulk density; therefore, increased powder bed density is expected during PBF-LB processing (see Figure 5b,c), likely by reducing interparticle friction and allowing for better powder packing. This improved packing can lead to more uniform porosity within the part volume. However, the melting and solidification dynamics during PBF-LB also play a crucial role in determining the specific shape of pores—such as the formation of more spherical pores.[18,22]

Interestingly, Ag NP-modified powders exhibit higher porosity with larger, spherical pores, a phenomenon typically expected to reduce the UTS due to the presence of stress concentrators.[69] However, the UTS for Ag-modified samples is increased (Figure 5f). This counterintuitive result suggests that additional factors—such as altered crystallinity, improved NP distribution, or modifications to the polymer matrix during melting—may compensate for the improvement in strength despite the increased porosity. However, CB-modified PA12 powders improve sintering efficiency by increasing heat conductivity with better laser heat absorption, resulting in less porosity and finer pores than parts made out of unmodified PA12 powders.[73] This highlights the complexity of the process and the intricate interplay between NP modification and the resultant material properties.

PC3 captures 9.8% of the variance in the polymer powder dataset, with loadings primarily influenced by the D10 powder size

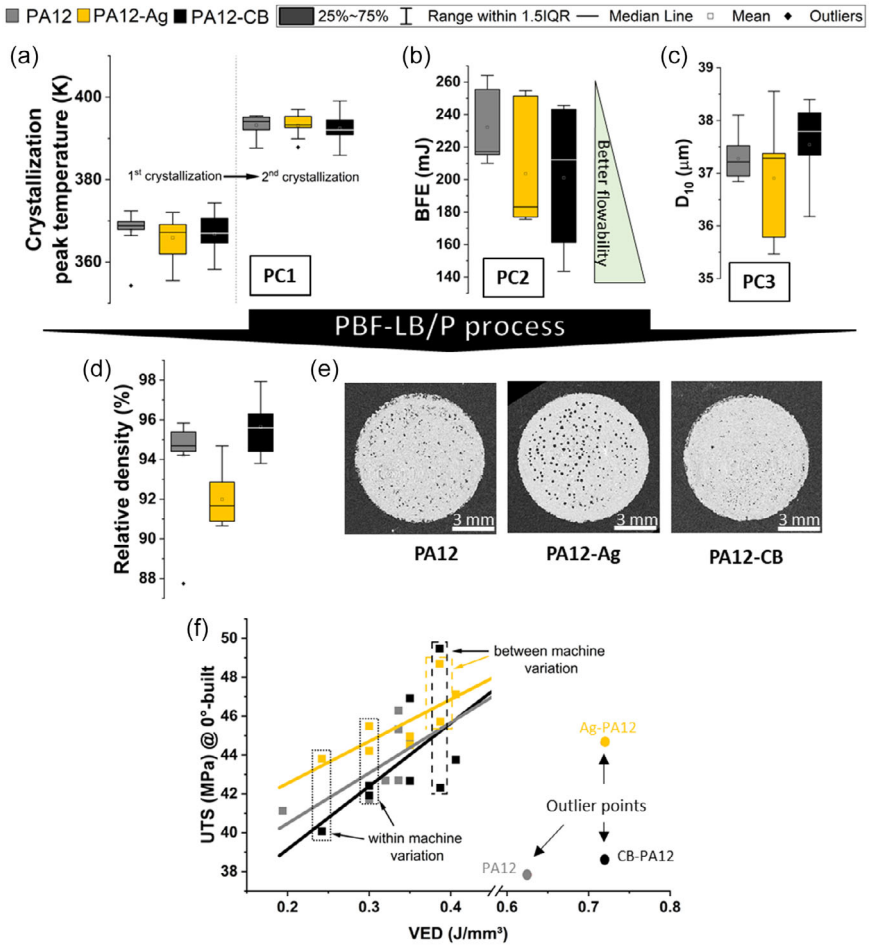

Figure 5. Powder properties of PA12-based feedstocks: a) crystallization temperature, b) basic flowability energy, and c) D_{10} powder size; and structural properties of PA12-based as-built parts: d) relative density, e) micro-CT cross-section images showing pore morphology and distribution, and f) UTS at horizontal (0°) build direction for the studied VED range.

(Figure 3c). The PC3 scores are higher for CB-modified powders and lower for Ag-modified powders than commercial powder. This trend is supported by the D_{10} property data shown in Figure 5c. The D_{10}, D_{50}, and D_{90} values for both modified powders (see also Figure S5 in the Supporting Information) were lower than those of commercial PA12. However, the observed changes are minimal (<1 µm), below the precision limit of the applied measurement method, namely, laser diffraction, where computer software interprets the light scattering data to calculate the most likely size distribution.[74] While this demonstrates the sensitivity of the PCA, it also indicates that the data require careful interpretation to avoid overestimating minor differences.

Overall, the PCA reveals numerous correlations between powder properties, highlighting the complex interactions in the PBF-LB process given by the vast cumulative correlations described in the introduction. Although PCA effectively identifies key variables affecting material properties, the complex relationships are not always clear. For example, NP modifications subtly impacted crystallinity, flowability, and mechanical properties, sometimes yielding unexpected results such as increased UTS despite increased porosity, as observed for the Ag-modified as-built polymer parts. Due to the complexity of the PBF-LB process chain, an ML approach is used to analyze the entire process. This advanced analysis aims to uncover hidden correlations, offering deeper insights and potentially new avenues for process optimization.

2.3. Establishing Powder, Process, and Property Relationships along the Entire PBF-LB Process Chain via ML and Posthoc Model-Agnostic Techniques

PCA revealed the statistically most strong descriptors across various feedstocks, yet the complexity of the process restricted direct associations with part properties. To overcome this, we exploit ML models to predict the as-built part features for metals and polymers using feedstock properties and processing parameters. Incorporating the PCs from the PCA as input for these models has been an effective strategy, as the PCs captured the most significant variations in powder properties, reducing dataset dimensionality and complexity. In total, the ILS yielded

46 (metals) and 32 (polymers) output part features, and a subset of those have been chosen for further ML processing. Due to the lack of available data points in the data matrix, some part features are excluded, which are named in Table S5 and S6 in the Supporting Information. This approach emphasized critical powder characteristics while minimizing noise, enabling the models to focus on the main factors affecting part properties.[75] Thus, the inputs to the ML models are the PCs representing feedstock characteristics (6 and 10 PCs for metals and polymers, respectively, capturing 90% of the variation in powder data) and PBF-LB process features (7 each for metals and polymers, see Table S7, Supporting Information). The output of ML is the feature representing the microstructure and mechanical properties of the as-built parts.

In this study, we explored two ML models for establishing quantitative relationships between the powder properties, process parameters, and the measured as-built part properties: 1) linear ensemble LASSO (eLASSO) and 2) nonlinear ensemble support vector regression (eSVR) (details are provided in the Experimental Section). As shown in Figure S6 in the Supporting Information, the nonlinear eSVR models consistently outperformed the linear eLASSO models. Aware that eSVR models are "black-box" and lack intrinsic interpretability, we employed two model-agnostic posthoc explanation techniques—global feature importance (GFI) and overall interaction strength (OIS)—to gain insights into the learned patterns. Results from these analyses are visualized in **Figure 6** for metals and polymers, respectively. Additional details are given in the Experimental Section.

A feature with a GFI value close to 1 is considered critical for the prediction in isolation, while a low GFI score indicates limited standalone significance. According to Figure 6, PC1 (dominated by bulk density and flowability) is relatively low in importance for predicting as-built properties in metals. For polymers, PC1 and PC2 (influenced by crystallization temperature II, bulk density, and flowability) similarly show low individual contributions. The GFI analysis quantifies the importance of individual input features on the eSVR. However, OIS results show that these same features (PC1 for metals, and PC1 and PC2 for polymers) exhibit high interaction strength with other output variables, suggesting that while these features may not individually drive predictions (as GFI indicates), they significantly contribute when interacting with other features. This outcome is particularly relevant to the PBF-LB process, where process

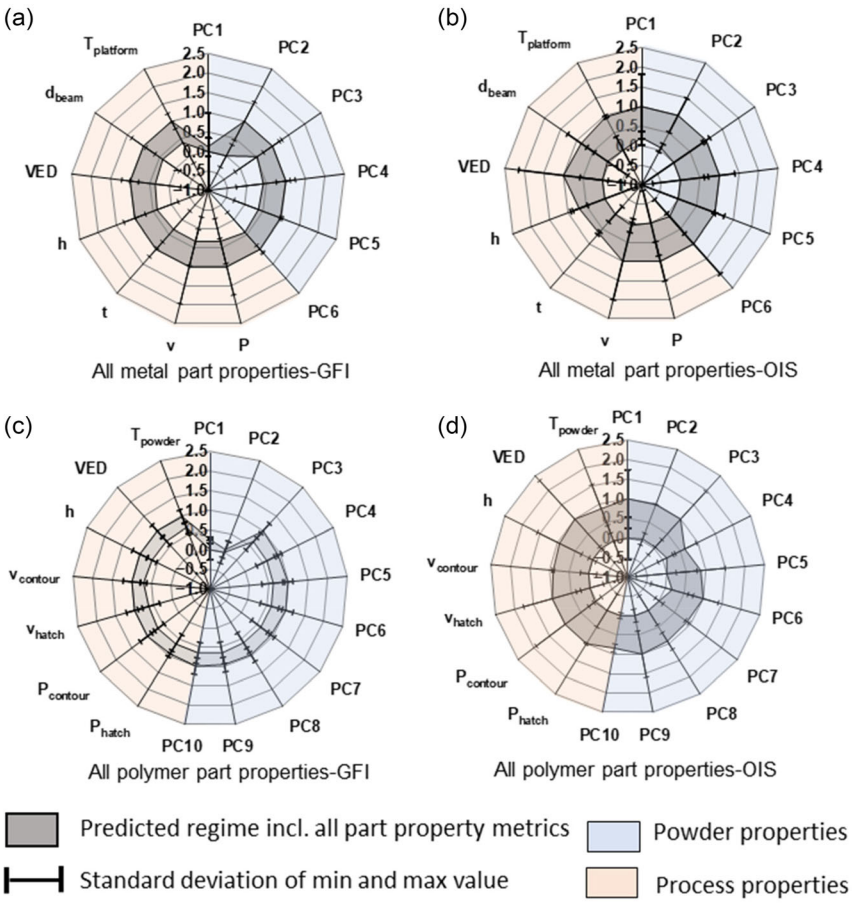

Figure 6. Radar charts representing the variable importance of each input feature as learnt by the trained eSVR models. a,b) The two radar charts summarize all 37 as-built properties, including commercially and NP-modified AlSi10Mg-based metal parts; c,d) all 28 as-built properties including commercially and NP-modified PA12-based polymer parts. (a,c) GFI and (b,d) OIS were normalized so that the minimum and maximum values are rescaled to 0 and 1, respectively.

characteristics and powder properties are interdependent and seldom act in isolation. For example, improved bulk density reduces the voids between particles, which must be filled during the coalescence, interacting with crystallization temperature in polymers that influence the material's densification behavior under thermal processing.[27] Thus, in PBF-LB, understanding how parameters interplay is critical, as isolated consideration of features (as GFI does) cannot capture the inherent complexities and interdependencies of the full process chain.

In summary, both GFI and OIS analyses are indispensable for revealing the multilayered dependencies in PBF-LB. High OIS scores combined with low GFI for certain features emphasize the significance of interactions within the model, reflecting the real-world complexity of the PBF-LB process. This study, therefore, focuses primarily on the OIS results to capture these practical, interaction-driven insights. However, to retain valuable information on individual feature contributions, the GFI results are included in the Supporting Information (see Figure S7–S15, Supporting Information) for those interested in examining isolated effects. Key outcomes from the OIS analyses for specific as-built properties are summarized in **Table 1**. It reveals which process parameters and powder properties are essential to understanding the variations in part properties. The OIS results demonstrated how the properties of metal and polymer parts depend on powder and process characteristics, which behave differently throughout the entire PBF-LB process chain. Additionally, NP modification is crucial in tuning powder properties and influencing microstructural properties. While we were able to extract generic trends (i.e., identify important powder properties and PBF-LB processing parameters as learnt by the eSVR models), two factors prevent us from making conclusive statements about the correlations for individual structural part properties: 1) presence of large error bars in the GFI and OIS results (see Figure S7–S15 in the Supporting Information) and 2) lack of a similar study in the literature where the entire process chain has been investigated to correlate powder properties, PBF-LB processing conditions, microstructure, and as-built properties. In principle, the problem of large error bars can be addressed by sequential or adaptive learning using an iterative feedback loop.[76,77]

The eSVR models can recommend PBF-LB processing conditions that resulted in the largest uncertainty in the predicted part properties for further experimental investigation. The results from these experiments will enhance the dataset, allowing the eSVR models to be retrained for improved prediction performance and potentially better inference capabilities.

It is worth noting that the large error bars observed in the GFI and OIS results suggest that any effects of <0.5 wt% NP modifications on structural part properties are either too small to be reliably detected or generally minimal within the conditions of this study. Importantly, there are no indications of negative impacts from NP modifications, a critical requirement for industrial applications. While the structural properties of as-built parts do not appear to be significantly influenced by <0.5 wt% NP modification with the used nanomodification techniques in ILS for the studied materials of AlSi10Mg alloy and PA12, this does not preclude the potential functional benefits NPs can provide. Depending on the application, NPs could enhance material properties such as thermal conductivity or tailored magnetic performance.[63,78] These functionalities were not the focus of this study, which primarily investigated structural characteristics, but they represent a interesting area for future exploration.

A key takeaway from the ML approach is that complex, nonlinear relationships significantly influence powder properties,

Table 1. Summary of key eSVR results based on the OIS posthoc model explanation method for the metal and polymer dataset. The detailed results are shown in Section S3.1. in the Supporting Information. The OIS results are shown as input feature1: input feature 2 (e.g., PC3: hatch spacing). Input feature 1 has the strongest overall interaction with all other features, while input feature 2 is the feature that interacts most strongly with feature 1. Vertical yield strength refers to yield strength of samples built in vertical direction.

Materials	As-built part features	OIS
Metals	(Volumetric) relative density	• PC3:hatch spacing • PC3:PC2 (see Figure S7, Supporting Information)
	Total number of pores	• VED:laser beam diameter • VED:PC1 (see Figure S8, Supporting Information)
	fraction of LAGBs	• PC2:PC3 • PC2:platform temperature (see Figure S11, Supporting Information)
	Vertical yield strength	• Scanning speed: Powder layer thickness • Scanning speed: VED (see Figure S9, Supporting Information)
	Vertical elongation	• PC6:PC3 • PC6:PC4 (see Figure S10, Supporting Information)
Polymers	(Volumetric) relative density	• Powder bed temperature:PC2 • PC3:PC2 (see Figure S12, Supporting Information)
	Polydispersity index (measure of broadness of molecular weight)	• VED:laser power hatch • VED:PC5 (see Figure S15, Supporting Information)
	Build job yield strength	• VED:PC3 • VED:laser power hatch (see Figure S13, Supporting Information)
	Build job elongation	• Laser power hatch:VED • Laser power hatch:scan speed (see Figure S14, Supporting Information)

PBF-LB processing conditions, microstructure, and part properties. While PCA provided a basis by identifying key powder and process variables, ML extended this analysis by revealing interaction-driven effects, emphasizing the necessity of understanding interdependencies between features rather than isolated effects. Posthoc model explanation analysis of eSVR results (summarized in Table 1) reveals that the powder properties and processing parameters interact to affect the part properties. An important characteristic of the ML approach is its predictive capability; given the powder properties and PBF-LB processing parameters, the trained eSVR models are equipped to predict the properties of as-built parts, along with the associated uncertainties. For example, strong interactions between scanning speed and powder layer thickness were identified as critical factors influencing the yield strength of metal parts built in vertical direction (see Figure S9, Supporting Information). Similarly, in polymers, the combination of powder bed temperature and key powder characteristics (PC2 and PC3) significantly affected the volumetric relative density (see Figure S12, Supporting Information). These findings highlight parameter combinations that require targeted experimental validation to further refine and optimize the PBF-LB process. Although prediction was not the central focus of this ILS study, the methodology demonstrates the potential of ML to support process optimization and material design. By focusing on such interaction effects, future studies could reduce uncertainties in the dataset and enhance the predictive robustness of the ML models, enabling a more comprehensive understanding of PBF-LB processes. Furthermore, the insights gained from this study suggest that NP-modified AlSi10Mg and PA12 feedstocks, while not altering structural part properties significantly, do not compromise them either. This neutral behavior lays a strong foundation for leveraging NPs to add functionalities to materials without negatively impacting their mechanical performance. Building on these findings, future research should explore the impact of NP modifications on nonstructural properties like thermal conductivity[63] or magnetic performance,[78] paving the way for broader applications in PBF-LB. Moreover, integrating sequential learning frameworks into future ILSs could further refine model predictions, uncover additional hidden relationships, and enhance the overall understanding of PBF-LB processes.

2.4. Capturing Dimensionless Figures of Merit along the Entire PBF-LB Process Chain of Metals and Polymers

In the previous two sections, we discussed how PCA and ensemble ML techniques uncovered several hidden correlations within the PBF-LB process, revealing key interactions between various powder-based latent variables (PCs) and process parameters. Despite demonstrating good predictive performance, one limitation of the eSVR approach is that these models could be more coherent. Although posthoc model explanation techniques such as OIS provided a formal framework to probe the blackbox eSVR models and unveil key input features, they do not directly offer a physical interpretation of the PBF-LB process. While these shortcomings can be addressed by incorporating adaptive learning and symbolic regression with posthoc explanation techniques,[79] exploring such strategies is beyond the scope of this article.

To complement the ML approach, we leverage dimensionless figures of merit to enhance our understanding of the complex interactions within the PBF-LB process in the as-built parts of both metals and polymers. As mentioned, the PBF-LB process involves interdependent material properties that seldom act in isolation, presenting a complex challenge. In the following, we will introduce dimensionless figures of merit to simplify these physical interdependencies and make them universally comparable. In general, dimensionless figures of merit reduce the number of variables by combining multiple independent parameters, facilitating analysis, and helping to identify dominant effects. Unlike the ML models, where a series of hyperparameters should be specified and optimized by data practitioners empirically, the dimensionless figures of merit encode domain-inspired physical principles in a linear or nonlinear functional form. They are based on deductive reasoning. In sharp contrast, ML methods rely on inductive reasoning. The idea of dimensionless figures of merit has been recognized in the AM literature.[80,81] For instance, the specific laser power, defined by factors such as absorptivity, laser power, scan speed, and material properties, combines aspects of the Péclet and Nusselt numbers to characterize heat transfer dynamics in the melt pool.[82] This dimensionless formulation allows researchers to investigate the relationship between energy input and resultant features such as porosity, melt pool depth, and melt track stability. Expressing these relationships in dimensionless form enables a more transparent and universal understanding of the PBF-LB process, independent of specific materials, thereby enhancing predictive capabilities and process optimization.[44,50,83–85]

From a mathematical perspective, dimensionless figures of merit can be derived from independent variables, where their units cancel out during calculations. The Buckingham Π theorem can be applied to facilitate this process. More details can be found in the Experimental Section. During the ILS, we encountered several independent variables, such as powder density (ρ), scan speed (ν) length (=layer height) (l), laser power (P), platform temperature (Θ), mechanical strength (σ), and specific heat (c), which, following the Buckingham π theorem, can be connected to (in total) 4 dimensionless figures of merit. It is essential to specify their context for parameters like density and length. In this study, density refers to the bulk density, and length represents the layer thickness. To ensure meaningful correlations, we selected definitions that best captured the observed dependencies between dimensionless figures of merit and the experimental results. ν, l, P, and Θ are process parameters, ρ, σ, and c are material properties. It should be highlighted that we intended that these material properties do not describe the properties of the additively manufactured components but the typical properties of the bulk materials. Thereby, we can consider the influence of very different materials, like polymers, aluminum alloys, and steels, in dimensionless figures of merit. Hence, the dimensionless figures of merit are fully based on input parameters before any experimental PBF-LB investigation, so that they bear fully predictive character. Of course, material properties depend on the manufacturing processes and the resulting microstructures, but for this purpose, we select representative material properties from typical manufacturing processes. For aluminum alloy Al10SiMg (A360), we use the

yield strength in the die-cast state without artificial aging, which is about 170 MPa.[86]

From there, four different relationships that yield dimensionless figures of merit can be established. These parameters collectively encapsulate the thermal and mechanical characteristics of the PBF-LB process, significantly influencing both process efficiency and material behavior. Further details are provided in the Supporting Information.

Dimensionless figure of merit 1 (Π_1, heat transfer) reflects the efficiency of energy absorption by the material during the PBF-LB process. A higher value signifies greater energy absorption, which enhances melting efficiency, while a lower value indicates insufficient heat transfer or excessive process speed.

$$\Pi_1 = \frac{\Theta c}{\rho v^2} \tag{1}$$

Dimensionless figure of merit 2 ($\Pi_{2,}$ heat distribution number) captures the influence of thermal conductivity (K), platform temperature, density, process rate, and length on the heat transfer capabilities of the material. A higher value suggests that the material can effectively conduct heat, enhancing thermal uniformity during processing, while a lower value may indicate poor heat distribution, potentially leading to defects in the final product.

$$\Pi_2 = \frac{\Theta \mathrm{K}}{\rho v^3 l} \tag{2}$$

Dimensionless figure of merit (Π_3, strength effector number) relates the material's mechanical strength (σ) to its density and the square of the scan speed. A higher value suggests that the material demonstrates favorable mechanical strength in relation to its density and processing speed, which is critical for maintaining structural integrity in the final parts. Conversely, a low value may signal a risk of mechanical failure during or after the manufacturing process.

$$\Pi_3 = \frac{\sigma}{\rho v^2} \tag{3}$$

Dimensionless figure of merit (Π_4, melting energy utilisation establishes the relationship between input power, material density, and process parameters. A higher value indicates more effective energy utilization during the melting process relative to the material's properties and processing conditions. In contrast, a lower value may reveal inefficiencies in energy use, potentially compromising the quality of the printed components.

$$\Pi_4 = \frac{P}{\rho v^3 l^2} \tag{4}$$

Interestingly, the ratio of Π_1 and Π_2 yields the Péclet number, a well-known dimensionless figure of merit in AM (further details in the Supplementary Information).[79] This relationship highlights the interplay between energy absorption and thermal conductivity in the PBF-LB process. By separating the Péclet number into these two components, we gain a deeper understanding of heat transfer mechanisms and their role in melting efficiency. Analyzing Π_1 and Π_2 individually also enables targeted process optimization. A low Π_1 may indicate the need for energy input or material properties adjustments. In contrast, a low Π_2 suggests that improving the thermal conductivity of feedstocks (e.g., through NP modification) could enhance uniform heat distribution. This targeted approach fosters effective optimization strategies. However, it is important to recognize the theoretical limitations of these dimensionless figures of merit when used in the context of predictive models. Furthermore, this decomposition aids in comprehensive material characterization, facilitating the selection of optimal materials for specific applications and improving performance in AM processes. These dimensionless figures of merit are intended as a first step toward simplifying complex process dependencies and should not be viewed as standalone predictive metrics. It underscores the interconnectedness of thermal and mechanical properties, essential for developing high-quality materials. Ultimately, insights from Π_1 and Π_2 not only enhance our understanding of heat transfer dynamics in the PBF-LB process and provide practical avenues for optimization, material characterization, and predictive modeling, leading to improved performance and quality in final parts. Future work should focus on experimentally validating and refining these dimensionless figures of merit, including comparisons the powder layer's (thermo) physical properties with established physical principles, to ensure their broader applicability and reliability.

These established parameters have now been applied to the dataset generated within the ILS using four selected examples (**Figure 7**). Additionally, measurements from the literature, highlighted in green in Figure 7, have been incorporated to validate and contextualize the findings (circles for polymers taken from ref. [87] triangles for metals taken from ref. [88,89]. In the plot of the relative density of printed metal and polymer components from the ILS study versus Π_1, the values range between 50 and 300, with a notable concentration between 50 and 100 (see Figure 7a,b). All measured volumetric relative densities exceed 99.5% (metals) and 90% (polymers), indicating high-quality densification, as was indicated in the SOPs of this ILS.[52] These parts were produced using NP-modified or commercial metal feedstocks with varying printing parameters, reflecting the flexibility allowed in the ILS design. The relationship shown in the plot aligns with the understanding that Π_1 relates to energy absorption and melting efficiency in the PBF-LB process. The clustering of Π_1 values between 50 and 100 suggests this range represents an optimal energy absorption scenario, where sufficient melting occurs to achieve near-full densification without excessive overheating. This balance is critical for preventing defects such as porosity and ensuring the structural integrity of the printed parts. Furthermore, the plot provides valuable physical insights. It indicates optimal energy absorption; within the identified Π_1 range, energy is effectively utilized to achieve high densities while avoiding overheating. It underscores the importance of parameter tuning flexibility, as achieving specific Π_1 values can standardize quality across different machines and parameter sets, making Π_1 a valuable target parameter for controlling density in PBF-LB processes. Finally, the concentration of values around specific Π_1 ranges could signify an energy efficiency window, where energy is employed most effectively for melting and consolidation, impacting both cost-effectiveness and speed in industrial applications. Furthermore, Π_2 reflects the interplay between thermal

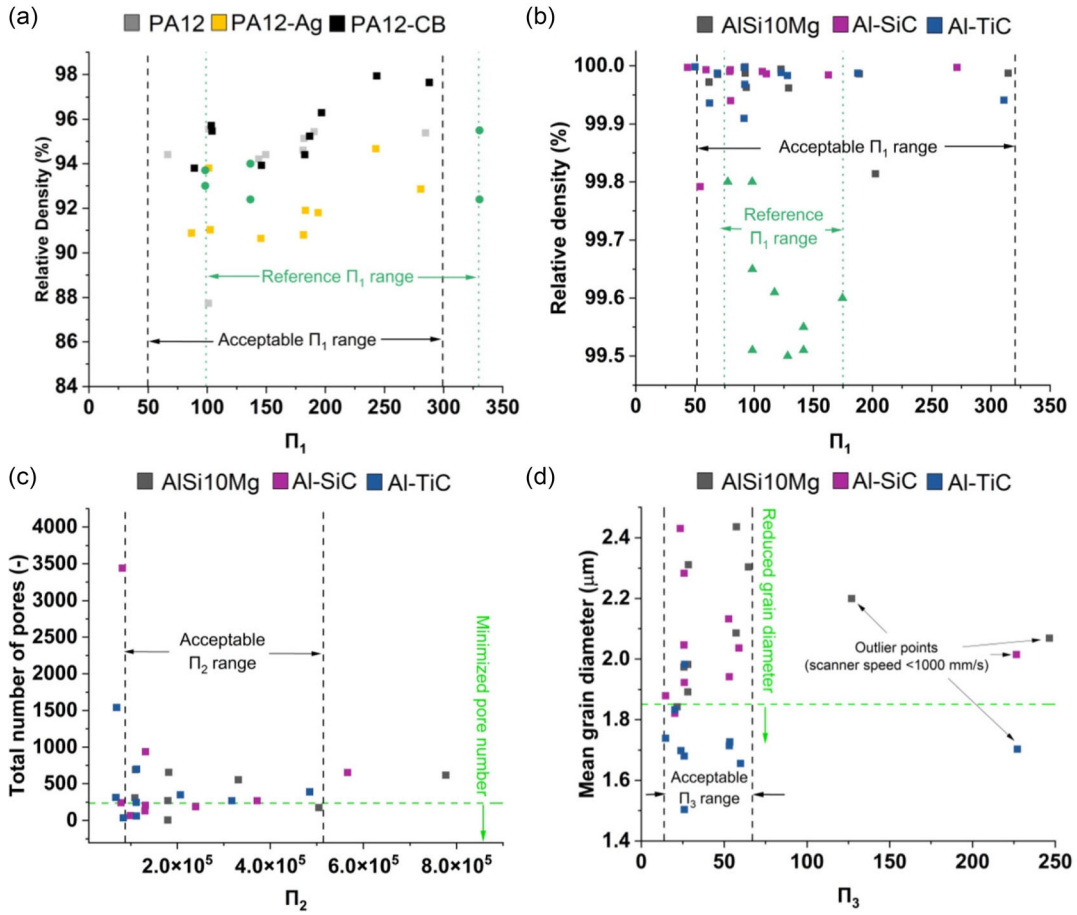

Figure 7. Dimensionless figures of merit versus as-built part properties for a) polymer and b–d) metal parts. Reference ranges validating the Figure of merits given between green dashed lines in (a,b) are extracted from the literature. Green circles correspond to polymer values taken from ref. [87], and triangles correspond to metal values taken from refs. [88,89]. The black dashed lines show the acceptable range for the investigated dimensionless figures of merit.

properties and process parameters, making it vital for understanding the PBF-LB process. Here, we decided to plot the volumetric total number of pores for metals, which is a highly underestimated parameter in PBF-LB literature (Figure 7c). By plotting pore counts against Π_2, we assess how effective heat distribution inside the powder bed influences melting behavior and solidification. The values for Π_2 center around 10^5, resulting in less than 500 pores within the investigated volume ($\approx 3.92 \times 3.92 \times 9.5\ mm^3$) per sample in this study. Π_3 relates the material's mechanical strength to its density and the square of the process rate (Figure 7d). For metals, the acceptable value range is found to be between 35 and 100 to obtain a mean grain diameter below 2.5 µm for commercial and SiC-modified ones and below 2 µm for TiC-modified AlSi10Mg. The set of dimensionless figures of merit Π_1–Π_4 provides a systematic framework for evaluating and optimizing PBF-LB processes, irrespective of the material system. While the current study focused on AlSi10Mg and PA12, the methodology can similarly be applied to other materials, such as polymer-based systems (e.g., TPU or LaB_6 NPs/TPU) or metal-matrix composites used in magneti PBF-LB. For instance, Π_1 and Π_2 can guide the selection of energy input and thermal conductivity parameters to ensure optimal melting behavior, while Π_3 and Π_4 help balance mechanical strength and energy utilization across varying process conditions.

Applying all four Π-numbers simultaneously offers a holistic approach to identifying recommended processing parameters. By analyzing their combined influence on the predicted part properties (e.g., density, mechanical strength, or grain structure), optimal corridors for scan speed, laser power, and powder layer thickness can be defined, even for novel material systems. This approach bridges the gap between input parameters and targeted outcomes, allowing researchers to predict suitable process settings based solely on feedstock properties and machine configurations as initially motivated. For example, in polymer PBF-LB, Π_1–Π_4 could help optimize parameters for materials with significantly different thermal properties, such as TPU. Here, Π_1 may reveal whether energy absorption is sufficient for uniform melting, while Π_2 could indicate the need for enhanced thermal conductivity, for example, through NP modification, to achieve consistent part quality. By providing a universal and material-independent framework, the dimensionless figures of merit enable systematic exploration of process-parameter spaces, offering actionable insights for new material systems and applications while reducing the reliance on trial-and-error approaches.

This comprehensive exploration of dimensionless figures of merit enhances our understanding of the PBF-LB process and highlights the need for further research into integrating these features with ML approaches. Future investigations could focus on how dimensionless figures of merit can guide the development of more coherent and interpretable ML models, ultimately leading to enhanced process optimization and material performance.

3. Conclusion

This study represents a milestone in systematically exploring the PBF-LB process for metals and polymers through an unprecedented ILS involving 32 international research institutions. By assessing six distinct feedstock types, including commercial and NP-modified AlSi10Mg and polyamide-12 (PA12) powders, the study comprehensively investigated the entire PBF-LB process chain. Over 1 200 000 correlations were extracted for 39 powder features, 7 process parameters, and 46 part properties of metal PBF and 30 powder features, 8 process parameters, and 32 part properties of polymer PBF. This vast dataset enabled an unparalleled evaluation of reproducibility, repeatability, and the role of feedstock properties in influencing process and part outcomes. The open-access dataset acquired under RDM standards defined in the SOPs, aligned with FAIR principles, offers a unique resource to bridge knowledge gaps and establish standardized protocols for consistent, high-quality production in AM. Beyond its immediate findings, this dataset serves as a foundation for exploring sustainability-focused innovations, such as reducing material waste and enhancing energy efficiency in PBF-LB processes.

The study highlights the promise of NP modifications, which improved powder properties such as bulk density, flowability, and thermal conductivity, contributing to enhanced microstructural and mechanical properties of as-built parts. However, reproducibility in as-built part properties was primarily limited in the metal parts, as the polymer components exhibited more consistent results. This emphasizes the critical need for defining tighter parameter corridors within the SOPs rather than solely monitoring compliance. Ensuring uniform adherence to these tighter corridors would help mitigate variability in process outcomes across laboratories. Importantly, the ability to process NP-modified powders without significant disturbances to the microstructure or mechanical properties of AlSi10Mg and PA12 demonstrates the flexibility of the PBF-LB process. This suggests that, in many cases, material properties can be tailored by nano-addtitives to meet specific functional requirements, such as improved corrosion resistance[39] or creep properties,[41] without the need for extensive reoptimization of process parameters. For example, with nanomodifiers below 0.5 wt%, the process can often proceed without requiring precompensated parameter adjustments, indicating a high degree of robustness of PBF-LB toward nanofunctionalized AM. For metals, NP modifications could additionally enhance properties such as thermal conductivity or electromagnetic behavior, enabling advanced functional applications.[90,91] For polymers, the functional enhancements may focus on bioactivity[88] or optical properties,[38,89] tailored to specific use cases. Furthermore, the use of NPs opens opportunities to manipulate phase transitions and interfacial interactions at the micro- and nanoscale, paving the way for advanced nanocomposite materials with superior multifunctional properties, such as 3D printing permanent magnets with high coercivity.[78] This underscores the broader utility of NP-modification in PBF-LB and highlights the potential for expanding material capabilities without compromising process reliability or repeatability.

Advanced statistical methods, such as PCA, and ML methods, such as eSVR, revealed hidden correlations and complex relationships within the dataset and proved powerful in extracting actionable insights from the dataset. PCA excelled in reducing dataset complexity and identified the dominant role of NP modifications in enhancing powder properties. At the same time, ML uncovered the interplay between powder characteristics and process parameters, highlighting key variability drivers. Posthoc model explanation techniques provided additional insights into critical input features influencing as-built part outcomes. These findings provide concrete guidance for parameter optimization and feedstock design. Furthermore, the developed four dimensionless figures of merit offer a physical framework for correlating powder, process, and part properties. These features simplify the complexity of PBF-LB, enabling universal comparisons across materials and conditions, thereby facilitating process optimization and offering predictive capability.

Future research should consider explicitly linking NP modifications to specific material classes and AM applications. For example, thermal and electromagnetic property enhancements could be integrated with metal printing applications, while bioactivity and optical properties could focus on polymers. Additionally, it would be valuable to reference established studies on nanodoped PBF processes to substantiate these claims or omit less evidenced effects. Furthermore, integrating dimensionless figures of merit with adaptive ML frameworks could further enhance predictive capabilities, optimize feedstock designs, and refine process parameters. Specifically, the experimental validation of dimensionless figures of merit in conjunction with advanced material characterization techniques, such as in situ X-ray diffraction or high-resolution electron microscopy, could provide deeper insights into the role of NP modifications in phase stability and defect evolution. While this large-scale study answered many questions along the process chain, it also opened the door for further, more specific investigations. The open-access dataset[51] invites the broader experimental, computational, and ML communities to build upon these findings, accelerating advancements in PBF-LB processes.

4. Experimental Section

Methodology to Generate ILS Data: A full version of the Experimental Section describing the feedstock modification, powder handling, characterization, processing, and part analysis can be found in the SOPs, published separately.[52] Machine types and printing parameters are given in Table S1 and S2 (SI). The following statistical and data-driven ML models were evaluated using the metal and polymer data matrix along the entire PBF-LB process chain generated with the experimental ILS dataset. The full dataset was open access e-published at DuEPublico.[51]

Reproducibility and Repeatability: The reproducibility of each measured powder, process, or part property feature was determined by calculating % RSD according to the formula below.

$$\%\,\mathrm{RSD} = 100 * s/|\bar{x}| \tag{5}$$

where s = the sample standard deviation and x = sample mean

Table 2. Conducted test methods and measured property features of powder, process, and part for virgin and NP-modified AlSi10Mg.

	Test method	Measured property features (unit*)
Powder	Ring shear	FFC (−), Bulk density (g m^{-3})
	Rotating drum	dAoR (°), CI (−)
	Karl–Fisher titration	Moisture content (ppm)
	DRIFTS	Laser Reflectivity (%)
	FT4 powder rheometer	BFE (mJ), FRI (−), CBD (−)
	Hausner ratio	Bulk density (g cm^{-3}), tapped density (g cm^{-3}), Carr index (%), HR (−)
	X-ray flourescence	Al (wt%), Si (wt%), Mg (wt%), Ti (wt%), Al/Si (−), Al/Ti (−)
	Optical emission spectroscopy	Al (wt%), Si (wt%), Mg (wt%), Ti (wt%) , Al/Si (−), Al/Ti (−)
	PSD by laser diffraction	D[10,3](μm), D[50,3](μm), and D[90,3] (μm)
	Dynamic image analysis	S (–), AR (−)
	DFSC	Tm[onset] (K), Tm[peak] (K), Tc[onset] (K), Tc[peak] (K)
Process	PBF-LB machine set	Laser power (hatch) (W), scanning speed (hatch) (mm s^{-1}), hatch spacing (μm), laser beam diameter (μm), powder layer thickness (μm), platform temperature (°C), VED (J mm^{-2})
Part	X-ray flourescence	Al (wt%), Si (wt%), Mg (wt%), Ti (wt%), Al/Si (−), Al/Ti (−)
	Optical emission spectroscopy	Al (wt%), Si (wt%), Mg (wt%), Ti (wt%) , Al/Si (−), Al/Ti (−)
	SEM-EBSD	Number of grains (−), mean grain diameter (μm), mean grain area (μm^2), max grain area (μm^2), and fraction of low-angle boundaries [fLAB(%)]
	PoreAnalyzer	Relative density (RD) (%), relative porosity (%), area median pore diameter (d50,2) (μm), span value of pore size distribution (σ) (−), max pore size (μm), area fraction of cracks (ppm), area fraction of gas pores (ppm), area fraction of unmelted partciles (ppm), and area fraction of lack of fusion (ppm)
	Optical microscope	Melt pool width (μm) and depth (μm)
	Micro-CT	Relative density (%), total number of pores (−), average pore size (μm), average pore volume (x105 μm^3), and average pore sphericity (−)
	Brinell hardness	Brinell hardness at building Z-Y/X (−) and scanning X-Y/Z direction (−)
	Tensile	UTS (σUTS), yield strength (σYS,0.2), elongation at break (%), and elastic modulus (E)

(*) (−) is dimensionless unit.

% RSD was calculated for powder, process, and part property features given in **Table 2** for virgin and NP-modified AlSi10Mg and in **Table 3** for virgin and NP-modified PA12.

Principal Component Analysis: An efficient analysis was essential to extract meaningful relationships from a dataset using ML models. A key step in this process involves reducing the dataset's dimensionality while minimizing the loss of important information. Various statistical techniques, such as PCA, can be employed for dimensionality reduction. The PCA approach reduces the dataset's dimensions while preserving as much data variance as possible.[75,92] The dimensions or the PCs calculated by PCA from the original dataset were expressed as a linear combination of all the features present in the data. For instance, the first PC (Z_1 or simply PC1) can be expressed as

$$Z_1 = \alpha_{11}X_1 + \alpha_{21}X_2 + \ldots + \alpha_{p1}X_p \quad (6)$$

Here, $X_1, X_2, \ldots, X_p$ are the features in the powder dataset and, $\alpha_{11}, \alpha_{21}, \ldots, \alpha_{p1}$ are known as the loadings for Z_1. For a dataset having p features, these loading vectors were calculated for all the PCs and mathematically expressed as our dataset's eigenvector of the covariance matrix. The eigenvector for the largest eigenvalue of the covariance matrix will correspond to the PC, explaining the largest variation in the dataset and is usually the first PC since the eigenvalues are arranged in descending order. Since eigenvectors are orthogonal to each other, the PCs were not correlated to each other. A dataset having n datapoints can be projected on this set of loading vectors to get the scores of the PCs for every datapoint. To determine the number of PCs for the reduced dataset, the cumulative variance explained by the PCs was plotted against their count. A 90% data variance cutoff was set for selecting PCs from PCA. The resulting input dataset for the ML models included the scores of the PCs that captured 90% of the variance in the original dataset. The prcomp() function from the stats library in R was used to perform the PCA on the dataset.[93]

Ensemble Learning: The basic idea of ensemble learning is to build a committee of data-driven models trained on independent datasets.[94] The final prediction for an observation will then be made by combining or aggregating the predictions from each individual model. In this approach, each model was assumed to be independent of the others, and the mean and standard deviation were calculated from the committee of models for a given property of interest. Among various ensemble learning methods, the bagging approach was employed. The original dataset consisted of n observations, and the bootstrap resampling technique was used to construct m replicas of n data points through sampling with replacement.[95] For LASSO, the value of m was fixed at 1000. However, for the SVR method, m was treated as a hyperparameter and optimized—along with two other hyperparameters discussed in the SVR subsection—using the 10-fold crossvalidation (CV) approach.

Support Vector Regression: Let $f(\boldsymbol{x})$ describe a linear function that maps the relationship between the inputs ($\boldsymbol{X}$) and an output ($\boldsymbol{y}$). The mathematical formulation of a linear SVR can be written in the form

$$\boldsymbol{y} = f(\boldsymbol{x}) = \langle \mathbf{w}, \boldsymbol{x} \rangle + \mathbf{b} \quad (7)$$

Table 3. Conducted test methods and measured property features of powder, process, and part for virgin and NP-modified PA12.

	Test method	Measured property features (unit)
Powder	Ring shear	FFC (−), Bulk density (g m^{-3})
	Rotating drum	dAoR (°), CI (−)
	Karl–Fisher titration	Moisture content (ppm)
	DRIFTS	Reflectivity (%)
	FT4 powder rheometer	BFE (mJ), FRI (−), CBD (−)
	Hausner ratio	Bulk density (g cm^{-3}), Tapped density (g cm^{-3}), Carr index (%), HR (−)
	X-ray flourescence	Ag (wt%)
	PSD by laser diffraction	D[10,3](μm), D[50,3](μm), and D[90,3](μm)
	Dynamic image analysis	S (−), AR (−)
DFSC	Tm[onset] (K), Tm[peak] (K), Tc[onset] (K), Tc[peak] (K)	
Process	PBF-LB machine set	Laser power (hatch) (W), scanning speed (hatch) (mm s^{-1}), laser power (contour) (W), scanning speed (contour) (mm s^{-1}) hatch spacing (μm), laser beam diameter (μm), powder layer thickness (μm), powder bed temperature (°C), VED (J mm^{-2})
Part	Micro-CT	Relative density (%), total number of pores (−), average pore size (μm), average pore volume (×105 μm^3), and average pore sphericity (−)
	Tensile	UTS (σUTS), yield strength (σYS,0.2), elongation at break (%), and elastic modulus (E)
	Oscillatory rheology	Complex viscosity at 1 Hz [Pa·s], Cross-over point frequency at 0.1% [Hz], Cross-over point dynamic modulus at 0.1% [kPa], LVE-strain limit at 1 Hz [%]
	Gel permeation chromatography	Number average molecular weight (Mn) (g mol^{-1}), the weight average molecular weight (Mw) (g mol^{-1}), and polydispersity index (PDI) (−)
	Gel permeation chromatography	Number average molecular weight (Mn) (g mol^{-1}), the weight average molecular weight (Mw) (g mol^{-1}), and polydispersity index (PDI) (−)

(*) (–) is dimensionless unit.

where $\boldsymbol{x}$ is an input vector of features, $\mathbf{w}$ are coefficients that fit the training data, and $\mathbf{b}$ is the intercept derived via the following optimization routine

$$\min \frac{1}{2}\|\mathbf{w}\|^2 + C\sum_{i=1}^{n}(\xi_i + \xi_i^*) \tag{8}$$

$$\text{subject to} \begin{cases} f(\boldsymbol{x}) - \langle \mathbf{w}, \mathbf{x}_i \rangle - \mathbf{b} \leq \in + \xi_i \\ \langle \mathbf{w}, \boldsymbol{x}_i \rangle + \mathbf{b} - \boldsymbol{f}(\boldsymbol{x}) \leq \in + \xi_i^* \\ \xi_i, \xi_i^* \geq 0 \end{cases} \tag{9}$$

where C is the regularization term, n is the total number of data points, $\in$ is the insensitive tube around the target values that provides the magnitude of the amount of permitted error (only those target values greater than $\in$ are penalized by the optimization), ξ_i, ξ_i^* are the nonnegative slack variables that permit a certain level of violation of the $\in$-tube bounds, and $\boldsymbol{x}_i$ is the descriptor for the i^{th} training data.[96,97] The regularization term C balances the model complexity and training error (large C and small C can lead to overfitting and underfitting, respectively). For a linear SVR, the kernel function, $\langle \mathbf{w}, \boldsymbol{x} \rangle$, is a dot product of $\boldsymbol{x}$ and $\boldsymbol{x}_i$, leading to a $\boldsymbol{f}(\boldsymbol{x})$ that is linear in $\boldsymbol{x}$. In this work, we used the nonlinear Gaussian radial basis function of the form.

$$\boldsymbol{\kappa}(\boldsymbol{x}, \boldsymbol{x}') = exp\left(-\frac{\|\boldsymbol{x} - \boldsymbol{x}'\|^2}{2\sigma^2}\right) \tag{10}$$

We determined the hyperparameters, C and σ, by CV from the training data to balance the bias–variance tradeoff. The hyperparameters that minimized the CV error were used for the final model. We performed this procedure for each model in this work. We used the function svm() from the e1071 library in R to perform the SVR regression.[98]

Like eLASSO, we combined the ensemble learning method with SVR, which we called eSVR. Since we do not know a priori how many bootstrap resamples (m) are needed to generalize our training data, we treated m as yet another hyperparameter. We considered four values of m: 25, 50, 75, and 100. Along with $\mathbf{C}$ and $\boldsymbol{\sigma}$, we also optimized for m using the 10-fold CV approach.

Global Feature Importance: With a large number of features for our dataset, the objective of GFI was to calculate the impact of individual features relative to other features on the predictions as learnt by the trained ML models.[99] To calculate the importance of a feature, the values of that feature were permuted, keeping the rest of the data the same, and then ML models were run to get the prediction on this new data. Mathematically, it is the difference between the prediction made with the original data and the prediction made with this new data having the permuted values for the feature. The predictions with new data should be less accurate if the feature is essential. It can be expressed as

$$V(f, i) = \overline{R}^i(f) - R(f) \tag{11}$$

Here, $\overline{R}^i(f)$ and $R(f)$ are the loss functions for the new data after permuting the $V(f, i)$ and the original data values, respectively. Loss functions are the measure of performance for the model and the performance after permuting the feature should go down if the feature is important. We used the function model_parts() from the DALEX package in R to implement this GFI method for ILS datasets.[100] Error bars were placed on the importance of the standard deviation of multiple bootstrap resamples used to

ensemble of ML models. For this work, 13 features were used for the metal dataset and 17 for the polymer dataset.

Feature Interaction via h-Statistics: As discussed earlier, the regression ML models comprise a set of features based on which the predictions are made. After GFI that captures individual feature importance on the predictions, we used Friedman's H-statistics to capture feature interactions and their impact on the predictions by the ML models.[101] We used two types of H-statistic values, which can be used to measure these OIS. The first one captured the interaction strength of one feature with all the other features at an instance. Mathematically it is expressed as

$$H_j^2 = \frac{\sum_{i=1}^{n} [F^i(x) - \hat{F}_j^i(x_j) - \hat{F}_{\setminus j}^i(x_{\setminus j})]^2}{\sum_{i=1}^{n} (F^i(x))^2} \tag{12}$$

Here, H_j^2 is the statistic that calculates the interaction of variable x_j with other variables and $F^i(x)$ is the prediction function value for a data point i from a dataset of total n points. Further, $\hat{F}_j^i(x_j)$ and $\hat{F}_{\setminus j}^i(x_{\setminus j})$ represent the average partial dependence of $F^i(x)$ on variable x_j and on all the other variables except x_j respectively. The second measure calculates the two-way interaction strength, which is more specific, and calculates the interaction strength between two specific features depending on how they affect the predictions. Mathematically

$$H_{jk}^2 = \frac{\sum_{i=1}^{n} [\hat{F}_{jk}^i(x_j, x_k) - \hat{F}_j^i(x_j) - \hat{F}_k^i(x_k)]^2}{\sum_{i=1}^{n} \left(F_{jk}^i(x_j, x_k)\right)^2} \tag{13}$$

Here, H_{jk}^2 is the measure to calculate the interaction between two variables; x_j and x_k and $\hat{F}_{jk}^i(x_j, x_k)$is the average partial dependency value of $F^i(x)$ on (x_j, x_k) combined where i is a data point from a dataset of total n points. Further, $\hat{F}_j^i(x_j)$ and $\hat{F}_k^i(x_k)$represent the averaged partial dependence of $F^i(x)$ individually on variable x_j and on variable x_k, respectively. The OIS and specific two-way interaction strength were calculated for all the features and plotted as bar charts. We had error bars on the interaction strength from the standard deviation of multiple bootstrap resamples used for our ensemble of ML models. These plots were generated for all the part property predictions to study the impact of feature interactions on them. We used the Interaction$new() function from the iml library in R to calculate these H-statistic values for our features.[102]

Supporting Information

Supporting Information is available from the Wiley Online Library or from the author.

Acknowledgements

The coordination office acknowledges financial support from the DFG under SPP2122 Project Number 359962234, "New Materials for Additive Manufacturing" and Evonik Industries for donation of the PA12 powder. As part of the SPP 2122, several subprojects contributed to this study and gratefully acknowledged labor and research units. The respective internal DFG project numbers were as follows: 409784234, 493935114, 409779181, 493947509, 410107213, 409791748, 493860861, 409485213, 493889809, 409766389, 409621284, 409726740, and 493892776. Besides the DFG SPP2122, external institutions in Germany technically supported the study within DFG project numbers 432804018 and 503259970. The authors also acknowledge the support of external and international research facilities and the technical assistance of Paul Spithill from the RMIT Advanced Manufacturing Precinct for technical investigation; Tim Robert Brocksieper from Hybrid additive manufacturing, Ruhr University Bochum for data curation, Johann Sokurov from the Institute of Technical and Macromolecular Chemistry, University Hamburg, for measurement execution and data mediation; Johannes Wilke from Otto Schott Institute of Materials Research, Friedrich-Schiller from University Jena for technical visualization; Stephanie Lippmann from Institute of Applied Physics, Friedrich-Schiller from University Jena for resources, methodology, and validation; Adam Whitbread from Centre for Additive Manufacturing, University of Nottingham for technical support; Nils Wiethoff and Daniel Christopher Behrens from Chair of Materials Science and Additive Manufacturing, University of Wuppertal for investigation and validation; Marco Martin Barreiros from Chair of Materials Technology, Ruhr University Bochum for technical apprentice; Rabia Yesiltas and Tinahan Tez from ALUTEAM, Fatih Sultan Mehmet University for technical coordination and validation; Guangxian Li from College of Polymer Science and Engineering, State Key Laboratory of Polymer Materials Engineering of China, Sichuan University for validation; Ömer Ersöz from Technical Chemistry I, UDE for sampling metal and polymer feedstocks; and Sylvia Monsheimer, Evonik, for her advice in the industrial board of the SPP2122, as well as Felix Müller, Evonik, for steadily supporting the networking activities

Open Access funding enabled and organized by Projekt DEAL.

Conflict of Interest

The authors declare no conflict of interest.

Author Contributions

Ihsan Murat Kuşoğlu: writing—original draft (equal); writing—review & editing (equal). **Sunidhi Garg**: writing—original draft (equal); writing—review & editing (equal). **Arvid Abel**: writing—original draft (equal); writing—review & editing (equal). **Prasanna V. Balachandran**: writing—original draft (equal); writing—review & editing (equal). **Stephan Barcikowski**: conceptualization (equal); data curation (equal); funding acquisition (lead); investigation (lead); methodology (equal); project administration (lead); resources (lead); supervision (equal); validation (supporting); writing—review & editing (supporting). **Louis Becker**: data curation (equal). **Jan-Simeon Bernsmann**: data curation (equal). **Jonas Boseila**: data curation (equal). **Christoph Broeckmann**: data curation (equal). **Mert Coskun**: data curation (equal). **Malte Dreyer**: conceptualization (equal). **Mark East**: conceptualization (equal). **Mark Easton**: data curation (equal). **Nils Ellendt**: data curation (equal). **Stan Gann**: data curation (equal). **Bilal Gökce**: data curation (equal). **Mareen Goßling**: data curation (equal). **Joachim Greiner**: data curation (equal). **Piotr Gruber**: data curation (equal). **Moritz Grünewald**: data curation (equal). **Kopila Gurung**: data curation (equal). **Nick Hantke**: data curation (equal). **Florian Hengsbach**: data curation (equal). **Hannes Holländer**: data curation (equal). **Brecht Van Hooreweder**: data curation (equal). **Kay-Peter Hoyer**: data curation (equal). **Yajiang Huang**: data curation (equal). **Florian Huber**: data curation (equal). **Olaf Kessler**: data curation (equal). **Burçin Özbay Kısasöz**: data curation (equal). **Stefan Kleszczynski**: data curation (equal). **Ebubekir Koc**: data curation (equal). **Tomasz Kurzynowski**: data curation (equal). **Arno Kwade**: data curation (equal). **Simon Leupold**: data curation (equal). **Dongmei Liu**: data curation (equal). **Felix Lomo**: data curation (equal). **Arne Lüddecke**: data curation (equal). **Gerrit A. Luinstra**: data curation (equal). **David A. Mauchline**: data curation (equal). **Fabian Meyer**: data curation (equal). **Lars Meyer**: data curation (equal). **Peter Middendorf**: data curation (equal). **Stefan Nolte**: data curation (equal). **Michał Olejarczyk**: data curation (equal). **Ludger Overmeyer**: data curation (equal). **Andrij Pich**: data curation (equal). **Sebastian Platt**: data curation (equal). **Felix Radtke**: data curation (equal). **Roland Ramm**: data curation (equal). **Silja-Katharina Rittinghaus**: data curation (equal). **Richard Rothfelder**: data curation (equal). **Johannes Rudloff**: data curation (equal). **Mirko Schaper**: data curation (equal). **Marie Luise Scheck**: data curation (equal). **Johannes Henrich Schleifenbaum**: data curation (equal). **Michael Schmidt**: data curation (equal). **Jan T. Sehrt**: data curation (equal). **Yvonne P. Shabanga**: data curation (equal). **Alexander Sommereyns**: data curation (equal). **Rabea Steuer**: data curation (equal). **Layla Shams Tisha**: data curation (equal). **Anastasiya Toenjes**: data curation

(equal). **Christopher Tuck**: data curation (equal). **Adrian Vaghar**: data curation (equal). **Bey Vrancken**: data curation (equal). **Zhengze Wang**: data curation (equal). **Sebastian Weber**: data curation (equal). **Jan Wegner**: data curation (equal). **Bai-Xiang Xu**: data curation (equal). **Yangyiwei Yang**: data curation (equal). **Duyao Zhang**: data curation (equal). **Evgeny Zhuravlev**: data curation (equal). **Anna R. Ziefuss**: conceptualization (equal); investigation (equal); methodology (equal); project administration (equal); supervision (equal); validation (lead); visualization (lead); writing—original draft (lead); writing—review & editing (equal). **Ihsan Murat Kuşoğlu** and **Sunidhi Garg** contributed equally to this work.

Data Availability Statement

The data that support the findings will be available in [Duepublico] at [https://doi.org/10.17185/duepublico/82674] following an embargo from the date of publication to allow for commercialization of research findings.

Keywords

additive manufacturing, AlSi10Mg, carbon black, laser powder bed fusion, machine learning, nanoparticles, PA12, repeatability, reproducibility, siliconcarbide, silver, selective laser melting, selective laser sintering, titaniumcarbide

Received: December 15, 2024
Revised: May 7, 2025
Published online: June 17, 2025

[1] D. Gu, X. Shi, R. Poprawe, D. L. Setchi, J. Zhu, *Science* **2021**, *372*, http://doi.org/10.1126/science.abg1487.
[2] E. M. Sefene, *J. Manuf. Syst.* **2022**, *63*, 250.
[3] M. Schmidt, M. Merklein, D. Bourell, D. Dimitrov, T. Hausotte, K. Wegener, L. Overmeyer, F. Vollertsen, G. N. Levy, *CIRP Ann. – Manuf. Technol.* **2017**, *66*, 561.
[4] F. Calignano, M. Galati, L. Iuliano, *Machines* **2019**, *7*, 72.
[5] E. D. Bain, *Polymer-Based Additive Manufacturing: Recent Developments* (Eds: J. E. Seppala, A. P. Kotula, C. R. Snyder), American Chemical Society, USA **2019**.
[6] L. Zhao, L. Song, J. G. Santos Macías, Y. Zhu, M. Huang, A. Simar, Z. Li, *Addit. Manuf.* **2022**, *56*, 102914.
[7] S. R. Narasimharaju, W. Zeng, T. L. See, Z. Zhu, P. Scott, X. Jiang, S. Lou, *J. Manuf. Process.* **2022**, *75*, 375.
[8] A. C. Bobel, A. K. Sachdev, T. W. Brown, *ASM Handbook Additive Manufacturing, Design, And Applications*, Vol. *24A* (Eds: M. Seifi, D. L. Bourell, W. Frazier, H. Kuhn), ASM International, Almere **2023**.
[9] M. White, J. Dobbs, *ASM Handbook Additive Manufacturing, Design, And Applications*, Vol. *24A*, (Eds: M. Seifi, D. L. Bourell, W. Frazier, H. Kuhn), ASM International, Almere **2023**.
[10] L. Judkins, G. Manogharan, R. Gupta, L. Jia, M. M. Tang, T. Teinturier, M. Hast, *ASM Handbook Additive Manufacturing, Design, and Applications*, Vol. *24A* (Eds: M. Seifi, D. L. Bourell, W. Frazier, H. Kuhn), ASM International, Almere **2023**.
[11] S. Chowdhury, N. Yadaiah, C. Prakash, S. Ramakrishna, S. Dixit, L. R. Gupta, D. Buddhi, *J. Mater. Res. Technol.* **2022**, *20*, 2109.
[12] R. Brighenti, M. P. Cosma, L. Marsavina, *J. Mater. Sci.* **2021**, *56*, 961.
[13] L. Cao, J. Li, J. Hu, H. Liu, Y. Wu, Q. Zhou, *Opt. Laser Technol.* **2021**, *142*, 107246.
[14] C. S. Abbott, M. Sperry, N. B. Crane, *J. Manuf. Process.* **2021**, *70*, 55.
[15] A. Raja, S. R. Cheethirala, P. Gupta, N. J. Vasa, R. Jayaganthan, *J. Mater. Res. Technol.* **2022**, *17*, 1013.
[16] S. Moylan, C. U. Brown, J. A. Slotwinski, *ASTM J. Test. Eval.* **2016**, *44*, 1009.
[17] B. Ahuja, A. Schaub, D. Junker, M. Karg, F. Tenner, R. Plettke, M. Merklein, M. Schmidt, *S. Afr. J. Ind. Eng.* **2016**, *27*, 30.
[18] T. Stichel, T. Frick, T. Laumer, F. Tenner, T. Hausotte, M. Merklein, M. Schmidt, *Opt. Laser Technol.* **2017**, *89*, 31.
[19] L. P. Lefebvre, J. Whiting, B. Nijikovsky, S. E. Brika, H. Fayazfar, O. Lyckfeldt, *Addit. Manuf.* **2020**, *35*, 101203.
[20] R. Pelletier, L. P. Lefebvre, B. Ludwig, T. Palmer, K. Brockbank, *Int. J. Powder Metall.* **2020**, *56*, 08887462.
[21] D. B. Hibbert, *Quality Assurance in the Analytical Chemistry Laboratory* (NY, 2007; Oxford Academic, 12 November 2020), https://doi.org/10.1093/oso/9780195162127.001.0001 (accessed: 28 October 2024).
[22] T. Stichel, T. Frick, T. Laumer, F. Tenner, T. Hausotte, M. Merklein, M. Schmidt, *J. Mater. Process. Technol.* **2018**, *252*, 537.
[23] C. U. Brown, G. Jacob, M. Stoudt, S. Moylan, J. Slotwinski, A. Donmez, *J. Mater. Eng. Perform.* **2016**, *25*, 3390.
[24] M. Schneider, D. Bettge, M. Binder, K. Dollmeier, M. Dreyer, K. Hilgenberg, B. Klöden, T. Schlingmann, J. Schmidt, *Pract. Metallogr.* **2022**, *59*, https://doi.org/10.1515/pm-2022-1018.
[25] C. L. Clark, E. K. Karasz, M. Melia, D. E. Hooks, R. Hackenberg, H. Colon-Mercado, P. Ganesan, P. Renner, S. Cho, M. Wu, S. R. Qiu, J. Dwyer, Z. Rueger, T. J. Gorey, Z. Koehn, J. A. Stull, *J. Manuf. Process.* **2023**, *106*, 380.
[26] V. N. Tondare, J. G. Whiting, A. L. Pintar, S. P. Moylan, A. Neveu, F. Francqui, *Powder Technol.* **2024**, *441*, 119810.
[27] C. A. Chatham, T. E. Long, C. B. Williams, *Prog. Polym. Sci.* **2019**, *93*, 68.
[28] Y. Wei, Y. Luo, Z. Wang, M. Peng, G. Li, Y. Huang, *Addit. Manuf.* **2024**, *79*, 103917.
[29] L. Haferkamp, L. Haudenschild, A. Spierings, K. Wegener, K. Riener, S. Ziegelmeier, G. J. Leichtfried, *Metals* **2021**, *11*, 418.
[30] M. Rahman, K. S. Islam, T. M. Dip, M. F. M. Chowdhury, S. R. Debnath, S. Md. M. Hasan, Md. S. Sakib, T. Saha, R. Padhye, S. Houshyar, *Prog. Addit. Manuf.* **2023**, *9*, 1197.
[31] A. Lüddecke, H. Zetzener, N. Hantke, A. Berger, M. Scheck, S. Weber, J. Sehrt, A. Kwade, *Powder Technol.* **2024**, *440*, 119790.
[32] J. Schmidt, W. Peukert, *Front. Chem. Eng.* **2022**, *4*, https://doi.org/10.3389/fceng.2022.995221.
[33] H. Chen, K. Kosiba, C. Suryanarayana, L. Tiwen, L. Yang, W. Yonggang, K. G. Prashanth, *Int. Mater. Rev.* **2023**, *68*, https://doi.org/10.1080/09506608.2023.2258664.
[34] E. Zhuravlev, B. Milkereit, B. Yang, S. Heiland, P. Vieth, M. Voigt, M. Schaper, G. Grundmeier, C. Schick, O. Kessler, *Mater. Des.* **2021**, *204*, 109677.
[35] I. M. Kusoglu, B. Gökce, S. Barcikowski, *Addit. Manuf.* **2020**, *36*, 101489.
[36] I. M. Kusoglu, C. Doñate-Buendía, S. Barcikowski, B. Gökce, *Materials* **2021**, *14*, 1169.
[37] I. M. Kusoglu, B. Gökce, S. Barcikowski, *Procedia CIRP* **2020**, *94*, 11.
[38] S. Heiland, B. Milkereit, K. Hoyer, E. Zhuravlev, O. Kessler, M. Schaper, *Materials* **2021**, *14*, 7190.
[39] N. Stratmann, M. Willeke, S. Leupold, M. Schmidt, S. Barcikowski, A. R. Ziefuss, *Procedia CIRP* **2024**, *124*, 69
[40] I. M. Kusoglu, P. Vieth, S. Heiland, F. Huber, A. Lüddecke, A. R. Ziefuss, A. Kwade, M. Schmidt, M. Schaper, S. Barcikowski, G. Grundmeier, *Procedia CIRP* **2022**, *111*, 10.
[41] S. Leupold, M. Willeke, C. Leong, N. Stratmann, A. Sommereyns, A. R. Ziefuß, S. Kopp, S. Barcikowski, M. Schmidt, *Procedia CIRP* **2024**, *124*, 61.
[42] N. Emminghaus, R. Bernhard, J. Hermsdorf, *Int. J. Addit. Manuf. Technol.* **2022**, *122*, 1679.
[43] A. Mussatto, R. Groarke, R. K. Vijayaraghavan, M. A. Obeidi, R. MacLoughlin, P. J. McNally, V. Nicolosi, Y. Delaure, D. Brabazon, *Mater. Chem. Phys.* **2022**, *287*, 126245.

[44] M. Grünewald, K. Popp, A. Chehreh, S. Gann, I. M. Kusoglu, S. Barcikowski, A. Nowicki, T. Schuffenhauer, M. Bastian, J. Rudloff, *AIP Conf. Proc.* **2024**, *3158*, 180001.
[45] M. Goßling, S.-K. Rittinghaus, S. Bharech, Y. Yang, M. B. Wilms, L. Becker, S. Weber, B.-X. Xu, B. Gökce, *J. Mater. Res.* **2023**, *39*, 774.
[46] P. Gabriel, J. Liu, F. Staab, T. D. Oyedeji, Y. Yang, N. Hantke, F. Scheibel, E. Adabifiroozjaei, O. Recalde-Benitez, L. Molina-Luna, Z. Rao, B. Gault, J. T. Sehrt, K. Skokov, B.-X. Xu, K. Durst, O. Gutfleisch, S. Barcikowski, A. R. Ziefuß, *ChemRxiv*, https://doi.org/10.26434/chemrxiv-2023-7pmp2.
[47] M. B. Wilms, S.-K. Rittinghaus, M. Goßling, B. Gökce, *Prog. Mater. Sci.* **2023**, *133*, 101049.
[48] C. Doñate-Buendía, D. Gu, M. Schmidt, S. Barcikowski, A. M. Korsunsky, B. Gökce, *Mater. Des.* **2021**, *204*, 109653.
[49] I. M. Kusoglu, F. Huber, C. Doñate-Buendía, A. R. Ziefuss, B. Gökce, J. T. Sehrt, A. Kwade, M. Schmidt, S. Barcikowski, *Materials* **2021**, *14*, 4892.
[50] A. Großmann, M. Rexer, M. Greiner, G. Meyer, J. Mölleney, L. Kohn, V. Abbatiello, P. F. Pelz, C. Mittelstedt, *Mater. Des.* **2024**, *238*, 112684.
[51] I. M. Kusoglu, S. Garg, A. Abel, P. V. Balachandran, S. Barcikowski, L. Becker, J.-S. Bernsmann, J. Boseila, C. Broeckmann, M. Coskun, M. Dreyer, M. East, M. Easton, N. Ellendt, B. Gökce, M. Gossling, J. Greiner, P. Gruber, M. Grünewald, S. Gann, K. Gurung, N. Hantke, F. Hengsbach, H. Holländer, B. Van Hooreweder, K.-P. Hoyer, Y. Huang, F. Huber, O. Kessler, B. Ö. Kısasöz, et al., *DFG SPP2122 Interlaboratory Study Dataset* **2025**, https://doi.org/10.17185/duepublico/82674.
[52] I. M. Kuşoğlu, A. R. Ziefuß, S. Barcikowski, Booklet for Standard Operational Procedures of DFG SPP2122 Interlaboratory Study measuring the effect of nanoparticles on the entire PBF-LB process chain of AlSi10Mg and PA12 **2025**, https://doi.org/10.17185/duepublico/82630.
[53] D. J. Huang, H. Li, *Mater. Des.* **2021**, *203*, 109606.
[54] M. Brandt, *Laser Additive Manufacturing-Materials, Design, Technologies, And Applications*, Woodhead Publishing, Darya Ganj, New Delhi **2017**, https://doi.org/10.1016/B978-0-08-100433-3.12001-9.
[55] J. A. Slotwinski, E. J. Garboczi, K. M. Hebenstreit, *J. Res. Natl. Inst. Standards Technol.* **2014**, *119*, http://dx.doi.org/10.6028/jres.119.019.
[56] A. B. Spierings, T. L. Starr, K. Wegener, *Rapid Prototyp. J.* **2013**, *19*, 88.
[57] F. Bittner, B. Müller, A. Echaniz, S. Matthes, B. Klöden, C. Kolbe, presented at *Lasers in Manufacturing Conf. 2021* **2021**.
[58] L. Dowling, J. Kennedy, S. O'Shaughnessy, D. Trimble, *Mater. Des.* **2020**, *189*, 108346.
[59] Y. Tan, J. Zhang, X. Li, Y. Xu, C.-Y. Wu, *Powder Technol.* **2021**, *393*, 154.
[60] N. Salem, S. Hussein, *Procedia Comput. Sci.* **2019**, *163*, 292.
[61] D. Riabov, L. Cordova, E. Hryha, S. Bengtsson, *Eur. J. Mater.* **2022**, *2*, 202.
[62] A. Lüddecke, O. Pannitz, H. Zetzener, J. Sehrt, A. Kwade, *Mater. Des.* **2021**, *202*, 109536.
[63] D. Gu, H. Wang, F. Chang, D. Dai, P. Yuan, Y.-C. Hagedorn, W. Meiners, *Phys. Procedia* **2014**, *56*, 108.
[64] O. Pannitz, A. Lüddecke, A. Kwade, J. Sehrt, *Mater. Des.* **2021**, *201*, 109530.
[65] O. Pannitz, F. Großwendt, A. Lüddecke, A. Kwade, A. Röttger, J. T. Sehrt, *Materials* **2021**, *14*, 3465.
[66] V. Lubkowitz, T. Scherer, V. Schulze, F. Zanger, presented at *Solid Freeform Fabrication 2023: Proceedings of the 34th Annual Inter. Solid Freeform Fabrication Symp. – An Additive Manufacturing Conf.* **2023**, https://doi.org/10.26153/tsw/50967.
[67] X. Liu, C. Zhao, X. Zhou, Z. Shen, W. Liu, *Mater. Des.* **2019**, *168*, 107677.
[68] R. Song, D. Ponge, R. Kaspar, D. Raabe, *Int. J. Mater. Res.* **2022**, https://doi.org/10.1515/ijmr-2004-0101.
[69] A. Sommereyns, T. Hupfeld, S. Gann, T. Wang, C. Wu, E. Zhuravlev, A. Lüddecke, S. Baumann, J. Rudloff, M. Lang, B. Gökce, S. Barcikowski, M. Schmidt, *Mater. Des.* **2021**, *201*, 109487.
[70] T. Hupfeld, A. Sommereyns, F. Riahi, S. Gann, M. Schmidt, B. Gökce, S. Barcikowski, *Materials* **2020**, *13*, 3312.
[71] C. Z. Yan, Y. S. Shi, J. S. Yang, J. H. Liu, *Rapid Prototyp. J.* **2011**, *17*, 28.
[72] T. Kigure, Y. Yamauchi, T. Nino, presented at *Inter. Solid Freeform Fabrication Symp., 2019*, University of Texas at Austin **2019**, http://dx.doi.org/10.26153/tsw/17319.
[73] J. Bai, R. D. Goodridge, R. J. M. Hague, M. Song, *Polym. Eng. Sci.* **2013**, *53*, 1937.
[74] S. J. Blott, K. Pye, *Sedimentology* **2006**, *53*, 671.
[75] M. Ringner, *Nat. Biotechnol.* **2008**, *26*, 303.
[76] P. V. Balachandran, *MRS Bull.* **2020**, *45*, 579.
[77] C. V. Headley, R. J. Herrera del Valle, J. Ma, P. Balachandran, V. Ponnambalam, S. LeBlanc, D. Kirsch, J. B. Martin, *J. Manuf. Process.* **2024**, *116*, 165.
[78] P. Gabriel, V. Nallathambi, J. Liu, F. Staab, T. D. Oyedeji, Y. Yang, N. Hantke, E. Adabifiroozjaei, O. Recalde-Benitez, L. Molina-Luna, Z. Rao, B. Gault, J. T. Sehrt, F. Scheibel, K. Skokov, X. Xu, K. Durst, O. Gutfleisch, S. Barcikowski, A. R. Ziefuss, *Adv. Sci.* **2024**, *11*, 2407972.
[79] A. Biswas, S. Liu, S. Garg, Md G. Morshed, H. Vakili, A. W. Gnosh, P. V. Balachandran, *MRS Commun.* **2024**, *14*, 983.
[80] T. Mukherjee, V. Manvatkar, A. De, T. DebRoy, *J. Appl. Phys.* **2017**, *121*, 064904.
[81] Z. Wang, M. Liu, *J. Mater. Process. Technol.* **2019**, *273*, 116238.
[82] Y. Yang, A. Großmann, P. Kühn, J. Mölleney, L. Kropholler, C. Mittelstedt, B. Xu, *J. Mater. Process. Technol.* **2022**, *299*, 117316.
[83] C. Bierwisch, *Materials* **2021**, *14*, 4530.
[84] M. Grünewald, K. Popp, J. Rudloff, M. Lang, A. Sommereyns, M. Schmidt, S. Mohseni-Mofidi, C. Bierwisch, *Mater. Des.* **2021**, *201*, 109470.
[85] C. Bierwisch, S. Mohseni-Mofidi, B. Dietemann, T. Kraft, J. Rudloff, M. Lang, *Procedia CIRP* **2020**, *94*, 74.
[86] *ASM Handbook, Volume 4E, Heat Treating of Nonferrous Alloys* (Ed: G. Totten), ASM International, Material Park, OH, USA **2016**.
[87] M. M. Lexow, M. Drexler, D. Drummer, *Rapid Prototyp. J.* **2017**, *23*, 1099.
[88] H. Hyer, L. Zhou, S. Park, G. Benson, B. Tolentino, B. McWilliams, C. Kyu, Y. Sohn, *Metallogr. Microstruct. Anal.* **2020**, *9*, 484.
[89] J. A. T. Rios, P. Zambrano-Robledo, J. D. T. Taborda, J. A. G. Espinoza, C. J. Isaza, A. Juárez-Hernández, *Int. J. Adv. Manuf. Technol.* **2023**, *129*, 3341.
[90] C. Doñate-Buendia, A. Ingendoh-Tsakmakidis, T. Hupfeld, A. Winkel, S. Barcikowski, B. Gökce, *Procedia CIRP* **2022**, *111*, 47.
[91] T. Hupfeld, A. Wegner, M. Blanke, C. Doñate-Buendía, V. Sharov, S. Nieskens, M. Piechotta, M. Giese, S. Barcikowski, B. Gökce, *Adv. Opt. Mater.* **2020**, *8*, 2000473.
[92] H. Hotelling, *J. Educ. Psychol.* **1933**, *24*, 417.
[93] R Core Team, R: A Language and Environment for Statistical Computing. R Foundation for Statistical Computing, Vienna, Austria **2021**, https://www.R-project.org/ (accessed: October, 2024).
[94] I. D. Mienye, Y. Sun, *IEEE Access* **2022**, *10*, 99129.
[95] B. Efron, *Breakthroughs in Statistics*, Vol. *2*, (Eds: S. Kotz, N. L. Johnson). Springer, New York **1992**, https://doi.org/10.1007/978-1-4612-4380-9_41.

[96] A. J. Smola, B. Schölkopf, *Statist. Comput.* **2004**, *14*, 199.
[97] H. Drucker, C. J. C. Burgers, L. Kaufmann, A. J. Smola, V. Vapnik, *Advances in Neural Information Processing Systems*, Vol. *9* (Eds: M.C. Mozer and M. Jordan, T. Petsche), MIT Press, Cambridge, MA **1996**.
[98] D. Meyer, E. Dimitriadou, K. Hornik, A. Weingessel, F. Leisch, _e1071: Misc Functions of the Department of Statistics, Probability Theory Group (Formerly: E1071), TU Wien_. R package version 1.7-13 **2023**, https://CRAN.R-project.org/package=e1071 (accessed: October 2024).
[99] G. König, C. Molnar, B. Bischl, *ArXiv*. https://doi.org/10.1007/978-3-030-68787-8.
[100] P. Biecek, *J. Mach. Learn. Res.* **2018**, *19*, 1.
[101] J. H. Friedman, B. E. Popescu, *Ann. Appl. Stat.* **2008**, *2*, 916.
[102] C. Molnar, G. Casalicchio, B. Bischl, *J. Open Source Software* **2018**, *3*, 786.